# Colloidal nanocrystals: Viable model systems for electronic quantum materials?

Jara F. Vliem, Jesper R. Moes, Ingmar Swart, and Daniel Vanmaekelbergh (✉)

*Debye Institute for Nanomaterials Science, Department of Chemistry, University of Utrecht, 3584 CS Utrecht, the Netherlands*

## ABSTRACT

The field of colloidal nanocrystals has witnessed enormous progress in the last three decades. For many families of nanocrystals, wet-chemical syntheses have been developed that allow control over the crystal shape and dimensions, from the three-dimensional down to the zero-dimensional case. Additionally, careful control of surface chemistry has enabled the prevention of non-radiative recombination, thus allowing the detailed study of confined charge carriers and excitons. This has led to a vast amount of applications of nanocrystals in displays, labels, and lighting. Here, we discuss how this expertise could benefit the rapidly advancing field of quantum materials, where the coherence of electronic wave functions is key. We demonstrate that colloidal two-dimensional nanocrystals can serve as excellent model systems for studying topological phase transitions, particularly in the case of quantum spin Hall and topological crystalline insulators. We aim to inspire researchers with strong chemical expertise to explore the exciting field of quantum materials.

## KEYWORDS

colloidal nanocrystals, topological insulators, quantum materials, edge/surface states

## 1 Nanocrystals as quantum materials

Semiconductor nanocrystals exhibiting quantum confinement in one or more dimensions (e.g. quantum dots, rods, platelets), have been a topic of intense research since their discovery over 40 years ago [1]. Due to quantum confinement effects, the emission spectrum of semiconductor nanocrystals can be accurately tuned by controlling their dimensions. This led to the belief that these nanocrystals might contribute significantly to display technologies [2]. Indeed, by the 1990s and early 2000s, pioneering studies began to explore how quantum dots could be integrated into light-emitting diodes and other displays [3, 4]. Since then, new wet-chemical synthesis techniques and breakthroughs in surface chemistry have enabled precise control over nanocrystal shapes and sizes, thereby significantly advancing the field of colloidal nanocrystals. These developments have resulted in the use of semiconductor nanocrystals in a wide variety of applications [5–9]. The success of nanocrystals in optoelectronics raises the question whether these materials could thrive in other areas of research as well. Here, we propose the use of colloidal nanocrystals in the next generation of electronic systems, in which energy-efficient transfer and processing of information is key. Specifically, we demonstrate how two-dimensional (2D) nanocrystals can serve as powerful model systems for investigating topological phases such as quantum spin Hall insulators and topological crystalline insulators. This review aims to highlight how the accumulated knowledge on colloidal nanocrystals can benefit the rapidly evolving field of quantum materials, encouraging researchers with a strong chemistry background to explore this field.

## 2 Nanocrystals, surface states, and surface chemistry

In addition to Alexei Ekimov and Louis Brus, who discovered that the absorption spectrum of nanometer-sized inorganic crystals reflects the confinement of the electron–hole exciton, Moungi Bawendi was the third researcher to receive the 2023 Nobel Prize in Chemistry [10]. Together with Chris Murray and David Norris, Bawendi developed a high-temperature, low growth-rate synthesis method for colloidal CdX (X = S, Se, Te) nanocrystals. By precisely controlling the reaction conditions, such as temperature and precursor concentrations, they were able to promote uniform growth. This control allowed the production of nearly monodisperse quantum dots that emit light from the lowest excitonic state [1, 11]. Consequently, the effects of particle-wave confinement in the nanocrystal host became observable, not only in the absorption, but also in the emission spectrum. Due to this confinement effect, which adds kinetic energy to the excited electron and hole pair (i.e. the exciton), the optical properties of nanocrystals can be tuned by controlling their size. The work conducted by Bawendi's group marked the breakthrough that led to substantial advancements in nanocrystal chemistry and a deeper understanding of the optoelectronic properties.

Besides size inhomogeneity, another significant challenge in nanocrystal synthesis is the presence of unpassivated surface states. Surface states are electronic states localized at the surface of nanocrystals that can trap excitons and reduce photoluminescence efficiency. I. Tamm [12] and W. Shockley [13] already showed in the 1930's that the termination of atomic periodicity results in an electronic state localized close to the terminating atom. Such a surface state has a different energy from the orbital states of the

interior atoms, and is therefore not part of a specific electronic band [13]. If this state is positioned in the band gap between the highest occupied valence band and the lowest empty conduction band, the exciton emission is often deteriorated by non-radiative recombination via this surface state. Due to the small size of nanocrystals, a relatively high number of atoms is situated at the surface. These surface atoms have a lower coordination than those in the bulk, and therefore they form energy levels that deviate in energy from the regular valence- and conduction bands [13, 14]. CdX nanocrystals, for instance, show dangling bond states on the surface Cd atoms. To solve this problem, Bawendi's group proposed to passivate the dangling bonds on the surface Cd atoms with a functionalized alkene (TOPO) [1]. This changes the environment of the Cd atoms at the surface to closely resemble that of the interior atoms in the zinc blende crystal. Consequently, the surface states shift towards the energy of the bands and do not affect the exciton photoluminescence. Due to the extensive chemical efforts by many brilliant chemists, the chemical passivation with organic ligands [15–21] and epitaxial inorganic shells [22–25] became state of the art (the cited publications just provide an impression and are far from complete). This not only resulted in high photoluminescence quantum yields, but also led to better shape and size control and a higher stability of the nanocrystal dispersion, enabling the self-assembly of nanocrystals into superlattice solids [26–30]. The understanding of how nanocrystal surface energies can be altered with surfactants—also during nanocrystal growth—resulted in a variety of shapes beyond quasi-spherical quantum dots, such as platelets (2D confinement), rods (one-dimensional (1D) confinement), or even rings and tetrapods [31–34]. Ligand exchange procedures further enabled functionalization and passivation of nanocrystals by the replacement of traditional organic ligands with inorganic ligands, for example making them dispersible in aqueous environments [18, 35, 36]. Due to the great advances in surface state passivation, many families of semiconductor nanocrystals nowadays show photoluminescence quantum yields between 50% and 100%, leading to practical applications in displays, TV screens, light-emitting devices (LEDs), and biomedical research [5–9]. For such applications, subtle surface chemistry has enabled the transfer of nanocrystals from the conventional non-polar solvents to the more polar solvents used in industry. Recently, there has also been a drive towards the development of more sustainable nanocrystal materials such as InP and CIS quantum dots [37–40].

It is evident that a good understanding of surface states has been crucial for nanocrystal applications [41–45]. However, an entirely different class of surface states, found in topological insulators (TIs), remains relatively unknown and underutilized. Unlike conventional surface states with a local chemical origin (see above), TI surface states originate from and are protected by the bulk band structure, resulting in unique electronic properties such as robust, spin-polarized conduction channels that are protected against non-magnetic impurity scattering. These non-scattering states could pave the way for new applications in the field of quantum materials, including advanced electronics, spintronics, and quantum computing. The extensive chemical expertise developed for manipulating nanocrystal surface states may now aid us in understanding and controlling topological surface states.

## 3 Topological surface- and edge states protected by the crystal band structure

To provide a basic understanding of topological insulators, we will start with a brief overview of their discovery and the theoretical principles behind them. Since it is not our aim to provide an in-depth theoretical basis of electronic topological insulators in the single-particle regime, nor to review the role of possible electron interactions in these systems, we refer the interested reader to excellent reviews on these topics [46–55].

A three-dimensional (3D) TI is a bulk insulator with metallic surface states characterized by a Dirac cone with spin-momentum locking, i.e. $(E, p, \downarrow)$, $(E, -p, \uparrow)$, and protected by time reversal symmetry (TRS) [56–58]. In 2007, the theoretical predictions of L. Fu, C. L. Kane, and E. J. Mele kickstarted the search for topological insulators [57]. Soon after the theoretical groundwork was laid, angle-resolved photoemission spectroscopy (ARPES) on $Bi_{0.9}Sb_{0.1}$ revealed the presence of a single Dirac cone on the material's surface, thereby confirming it as a 3D TI [59]. Bismuth selenide and bismuth telluride ($Bi_2Se_3$, $Bi_2Te_3$) later emerged as more promising TI candidates for applications due to their simpler band structure and larger band gap [56].

To understand the origin of the dispersive Dirac-type states present on the surfaces of three-dimensional topological insulator crystals, it is instructive to compare the family of $Bi_2X_3$ (X = S, Se, Te) bulk crystals [56, 60] to the well-known CdX (X = S, Se, Te) crystals. $Bi_2S_3$ is a trivial (non-topological) insulator: its valence band is formed from the frontier sulfur p-orbitals while its conduction band is predominantly formed from the bismuth p-orbitals. Such trivial insulators can be depicted as shown in Fig. 1, right-most panel. Similar characteristics are observed across the entire CdX family, where the conduction bands exhibit mostly cadmium s-orbital character. In contrast, $Bi_2Se_3$ and $Bi_2Te_3$ show a significant alteration in the band structure (Fig. 1, first panel). The interaction between the bismuth and selenium p-orbitals, influenced by crystal field effects and strong spin-orbit coupling, causes a crossing which inverts the character of the valence and conduction bands [56]. Due to the avoided crossing, a negative (inverted) band gap emerges. A $Z_2$ invariant can be calculated from the filled bands to distinguish trivial from non-trivial materials, for which in three dimensions there are four [57, 61, 62]. It is important to note that the conditions for band inversion are specific to the interior of the crystal. Consequently, as one approaches the boundaries of a topologically non-trivial material from its bulk, a transition occurs where the bands converge and touch. This closing of the band gap gives rise to a two-dimensional Dirac cone at the crystal surface. Due to this bulk-boundary correspondence, the conductive surface states are robust to non-magnetic disorder and defects.

In addition to three-dimensional TIs, two-dimensional TIs exist. Analogously to the three-dimensional case, a two-dimensional TI has an insulating interior. However, instead of a conducting surface state, one-dimensional metallic states described by Dirac lines occur at the crystal edges [63, 64]. These edge modes exhibit helical behavior, i.e. spin-momentum locking in counter-propagating modes at the edge of the crystal (see central panel of Fig. 1). In this quantum channel, impurity or lattice vibration-induced scattering of a mode is prevented since back-propagating channels with identical spin are absent (i.e. time reversal symmetry (TRS) is respected). Backscattering can only occur in combination with a spin flip, where the red mode converts into the blue mode, or vice versa (see Fig. 1, nanocrystal schematic). The energy-momentum dispersion of the surface state may depend on the atomic registry of the surface [65] or edge [66]. Two-dimensional TIs are commonly referred to as quantum spin Hall insulators (QSHI) due to the analogy with the quantum Hall effect, discovered in the 1980's [46, 67–69]. Also for two-dimensional materials, a topological $Z_2$ invariant can be obtained from the band structure. The quantum spin Hall effect generalizes the quantum Hall effect for spinful systems, in which the role of the magnetic field is replaced by spin-orbit coupling such that TRS is respected. This effect was first predicted for two-dimensional
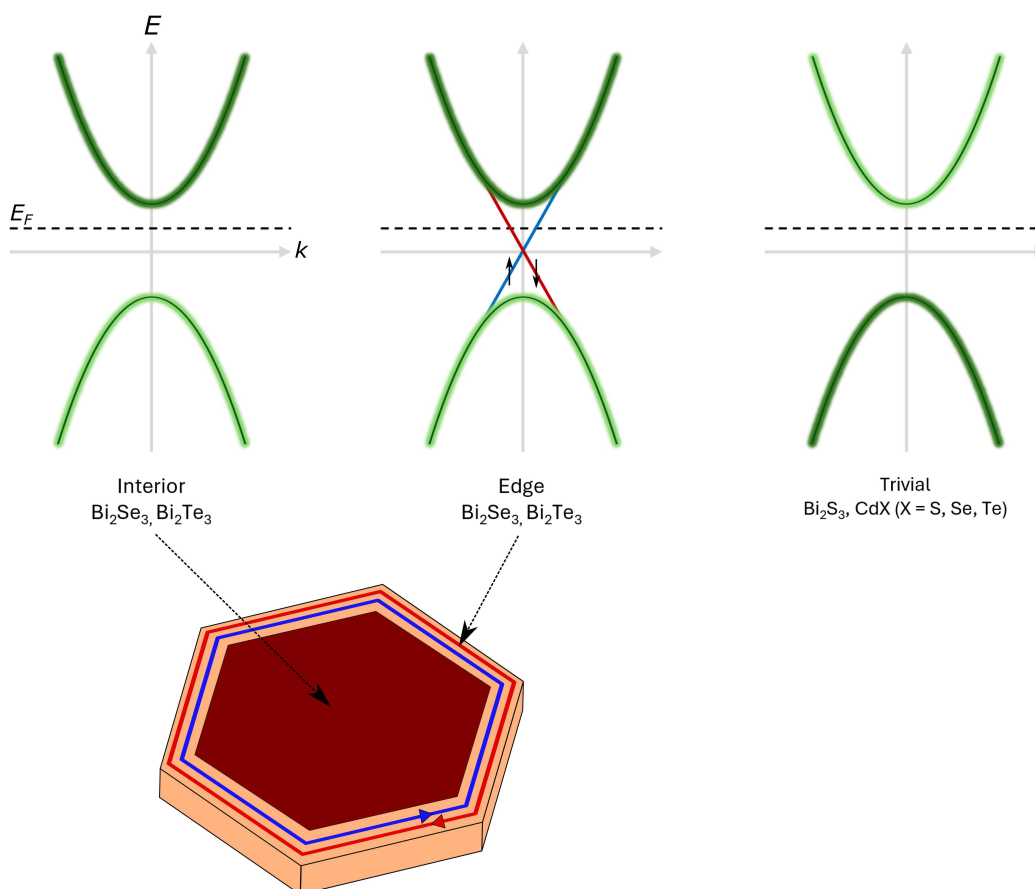
**Figure 1** Schematic band diagram of a trivial (non-topological) insulator and of a two-dimensional quantum spin Hall insulator with helical edge states. Top-right: the band scheme of the valence- and conduction band of a trivial insulator (such as CdSe nanoplatelets). Top-left: band scheme of $Bi_2Se_3$ as a quantum spin Hall insulator in which the valence and conduction bands are inverted and mixed (corresponding to the interior of a topological insulator). Close to the edge of a topological crystal, a pair of helical states (red: spin down, propagation clockwise; blue: spin up, propagation counter-clockwise) connect the valence and conduction band, see central band structure.

materials with a honeycomb geometry [64] (silicene, germanene, stanene) and for two-dimensional zinc blende HgTe quantum wells (thicker than 6 nm) sandwiched between CdTe layers [58]. Experimentally, the first results were reported for the HgTe/CdTe quantum well system. It was shown that edge states exist with a quantized conductance of $2e^2/h$ [70, 71]. Below, we will discuss the case of $Bi_2Se_3$, for which we have studied the transition from a three-dimensional to a two-dimensional topological insulator, both experimentally and theoretically.

In 2011 a different class of TIs was identified, namely that of the topological crystalline insulators (TCIs) [72]. In these materials, the point group of the crystal is explicitly included in the topological classification and band inversion is related to symmetries in the lattice that have direct consequences on the band structure [72–76]. The resulting conducting states in TCIs are thus mainly protected by the crystal symmetry (e.g. inversion and mirror symmetry). Since crystal symmetries are easily broken, TCIs only exhibit conducting states on highly symmetric surfaces. The requirement that the symmetry must be preserved in the surface layer makes this type of non-trivial topology vulnerable to distortions [77–79]. A well-studied class are crystals with a rock-salt lattice, such as SnTe [80–82] and $Pb_xSn_{1-x}Se/Te$ [83–91].

## 4  Devices based on topological insulators

As outlined in the previous section, the surface states of topological (crystalline) insulators result in robust, spin-polarized conduction. A 3D topological insulator has 2D conductive surface states, while a 2D topological insulator or quantum spin Hall insulator has 1D helical edge channels. In topological crystalline insulators, protected surface states only exist on high symmetry surfaces. These materials might find their use in a variety of electronic applications [92]. In general, the robust and dissipationless conduction may be of use in the development of devices that rely on surface conduction, such as transistors with non-backscattering surface-state transport channels or sensors. The development of such devices will require accurate surface engineering and material design in order to maximize the surface conductance. For instance, in $Bi_2Se_3$, the bulk conductance is often enhanced by inherent n-doping, which makes the contribution of the surface states to the overall conduction difficult to characterize [93–97]. Tuning of the Fermi level to ensure its location within the bulk bandgap, for example by doping or gating, is essential to ensure a surface-state dominated conduction and thus to prevent energy dissipation [60, 95, 98–103]. Moreover, as each surface channel will contribute a quantized conductance of $e^2/h$ [57], $n$ parallel helical channels are needed to increase the conductance to $ne^2/h$, which will require both helical edge states of limited width (< 20 nm), as well as the best of lithography and surface chemistry.

One major application of topological insulators is in the field of thermoelectric materials. Many well-known thermoelectric materials, such as $Bi_2Se_3$ and BiSb, were only later identified as topological insulators. Due to this discovery, recent research has focused on the effects of surface state (hybridization) and edge

states on the thermoelectric performance of TIs, which is characterized by the dimensionless figure of merit ZT = $\sigma S^2 T/\kappa$ [104–107]. Here, $\sigma$ is the electrical conductivity, $S$ is the Seebeck coefficient, $T$ is the absolute temperature, and $\kappa$ is the thermal conductivity. This formula shows how the high surface state conductivity of a TI could enhance thermoelectric performance. However, due to the curious interplay between surface states and bulk states, the exact way in which the two contribute to the thermoelectric performance is not trivial [108, 109]. It has also been shown that the reduction of bismuth chalcogenides to the nanoscale may enhance their figure of merit by effectively reducing the thermal conductivity $\kappa$ [110–112]. However, especially at the nanoscale, where hybridization effects start to play a role, many questions regarding the influence and interaction of bulk and surface states remain. For example, theoretical calculations have shown that the hybridization-induced gap that exists in the 2D limit could be tuned by adjusting the film thickness to effectively control the figure of merit [113]. The improvement of ZT by harnessing the topological properties of TIs remains an active area of research [114].

In addition to the use of topological insulator materials in thermoelectric devices, there are other, more exotic applications for these materials that are still in their infancy. For 2D TIs for instance, the robust helical channels should theoretically result in dissipationless electron transport. The helical modes provide direct access to direction-filtered spin channels (without the application of a magnetic field) making such TIs promising candidates in the field of spintronics. Experimental evidence for the existence of such helical channels has been presented [66, 70, 115, 116]. Furthermore, since the publication of the seminal work by Fu, Liang, and Kane (2008) [117], there has been ongoing research towards the experimental realization and detection of Majorana Zero Modes (MZMs), which could form the basis for topological qubits [117–125]. MZMs are quasiparticle states at zero energy that are expected show non-Abelian statistics, which is advantageous for quantum processing. These modes are predicted to occur at interfaces between topological insulators and superconductors [117]. Because of their topological origin, the quantum states depends on the global properties of the system rather than local perturbations, which should make them highly resistant to local sources of noise and error.

Despite the promising theoretical and experimental results, several challenges must be addressed to realize TI-based devices [92]. Besides the practicalities of device preparation, such as the growth of highly crystalline and functionalized materials with specific, well-tuned dimensions, there are still many open questions regarding the fundamental science behind topological insulators. As is the case for existing electronics, it is likely that TIs will be used on a nanometer scale. Because of this, investigation into the robustness of edge/surface states in T(C)Is with finite dimensions is required. Here, we will show how colloidal nanocrystals can be used for this purpose. Colloidal, solvent-based synthesis routes provide an unparalleled amount of freedom in the synthesis. This freedom can be used to obtain specific types of colloidal topological insulators with properties of interest, such as doped structures, core/shell structures, or colloids of various dimensions and shapes. As an example, we will present nanoplatelets of the bismuth-chalcogenide family as a model system to study the change in topological character when going from three to two dimensions. We emphasize that the finite lateral dimensions of two-dimensional $Bi_2Se_3$ in the shape of finite-sized nanoplatelets is a great asset in fundamental research. We will also introduce colloidal two-dimensional sheets of other chemical families that have been identified as TCIs. The dependence of the topological properties of TCIs on their crystal structure provides

additional flexibility that could benefit device design. Hence, TCI nanocrystals are important for studying how lattice distortions, symmetry, and dimensions impact topological properties. We will see that colloidal nanocrystals have important assets (but also drawbacks) with respect to MBE grown two-dimensional crystals.

## 5 Finite-size $Bi_2Se_3$ nanoplatelets as a model system to study (protected) edge states

In the last decade, many three-dimensional topological materials were grown by gas-phase deposition techniques, chemical vapor deposition and molecular beam epitaxy. The challenge is to obtain materials with a homogeneous thickness (large surface terraces, minor number of surface steps) and well-defined crystal-shape. In three-dimensional materials, the energy-momentum-spin relation of the surface states can be characterized by spin-resolved ARPES [126–128], providing a detailed picture of the filled valence bands and Dirac cone up to the Fermi-level. However, in two-dimensional QSHIs, edge states are more difficult to characterize. Characterization requires local scanning tunneling microscopy and spectroscopy on finite-sized crystals (i.e. with a size that is finite with respect to the scanning distances possible in a scanning tunneling microscope (STM)), with preferably a homogeneous thickness and a well-defined edge. Signatures of edge states were reported at surface steps of crystals grown by gas-phase deposition methods [129–132]. However, the measurement of a true edge state has only been possible recently, in $Bi_2Se_3$ nanoplatelets [66].

$Bi_2Se_3$ is a layered material with rhombohedral crystal structure consisting of (Se-Bi-Se-Bi-Se) layers called quintuple layers (QLs), separated by a van der Waals gap. $Bi_2Se_3$ crystals of > 6 QLs and large lateral dimensions can be considered as three-dimensional topological insulators with gapless surface states, while below 6 QLs, ARPES results have shown that hybridization of the surface states leads to the opening of a gap [133]. Up until recently it was unsure what exactly happens to the topological surface states when reducing the thickness of a 3D TI to make it two dimensional: is the resulting gap in the interior of the two-dimensional system still inverted and do we find a two-dimensional QSHI? Is there a one-dimensional quantum channel at the edge (see Fig. 1)?

Colloidal $Bi_2Se_3$ nanoplatelets have several assets that render them a valuable model system in this investigation [66]. First of all, the nanocrystals are self-standing and can be deposited on a substrate of choice for electrical scanning probe microscopy and spectroscopy, or even to prepare electrical devices. Secondly, the thickness of each platelet is uniform over the entire platelet, hence surface steps are absent and the edge termination of the two-dimensional crystal is well-defined (see Fig. 2). Thirdly, with lateral dimensions in the 100–200 nm range, the platelets can be classified as genuinely two-dimensional (i.e. there is no lateral confinement) and at the same time their finite dimensions allow scanning tunneling spectroscopy to investigate the interior of the crystal and the edge. Hence, all conditions are met that enable us to relate the insulating properties of the interior to the presence or absence of a quantum channel at the edge of the crystal.

Several papers have reported on the wet-chemical synthesis of $Bi_2Se_3$ nanoplatelets, which may have a reduced number of QLs (< 10) and lateral sizes in the 10 to 1000 nm range [94, 110, 134–147]. To control the thickness of the platelets (in unit number of QLs) together with the lateral dimensions of the platelets, we developed a hot injection method (to be published elsewhere). We were able to synthesize hexagonal $Bi_2Se_3$ platelets with a reasonably controlled thickness, i.e. the targeted number of QLs between 1 and 6 with an uncertainty of 1 QL, and lateral dimensions in the 100 nm range. Figure 2 shows the structural characterization of these platelets.
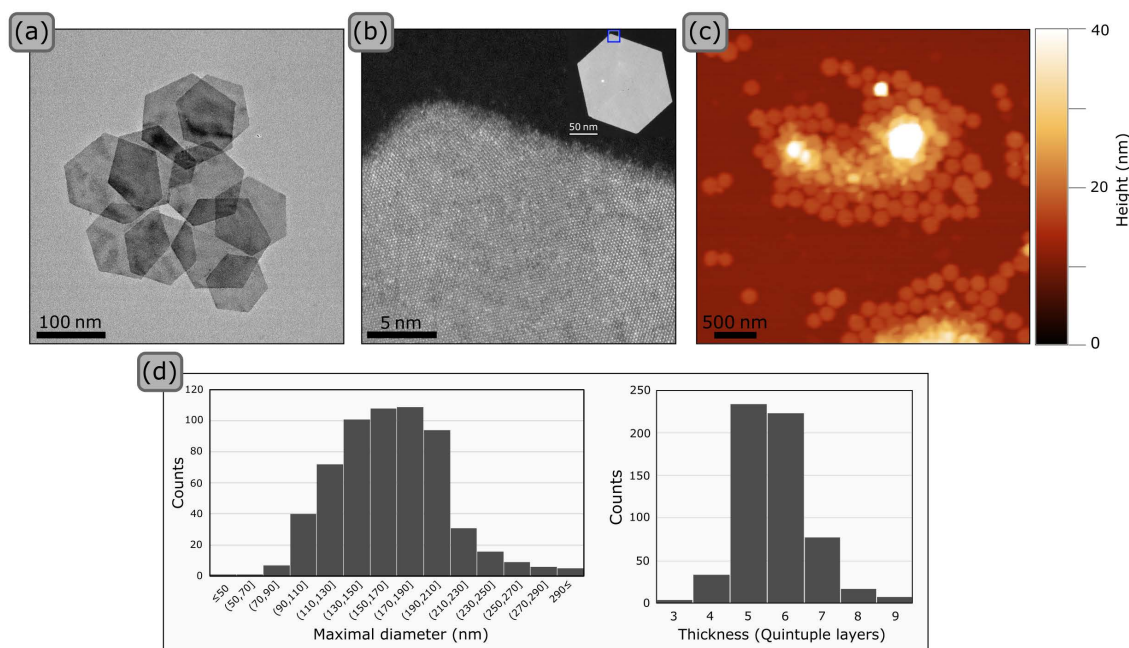
**Figure 2** Structural characterization of colloidal $Bi_2Se_3$ nanoplatelets prepared by a hot-injection method. (a) Transmission electron microscopy (TEM) image of an extract from a platelet suspension showing hexagonal platelets with a diagonal of approximately 150 nm. (b) High-angle annular dark-field scanning TEM (HAADF-STEM) image of the edge-corner region showing a slightly disordered edge region of 1 nm in width, and a crystalline (rhombohedral) crystal structure in the interior. (c) Example of an atomic force microscopy (AFM) picture used to measure the height and lateral dimensions of 700 platelets. (d) Diagrams of the distribution function of (left) the lateral size (cornet-to-corner diagonal), and (right) thickness (AFM height) of several batches of $Bi_2Se_3$ nanoplatelets. Images adapted with permission from Ref. [66], © Moes, J. R. et al. 2024. Further permissions related to the material excerpted should be directed to the ACS.
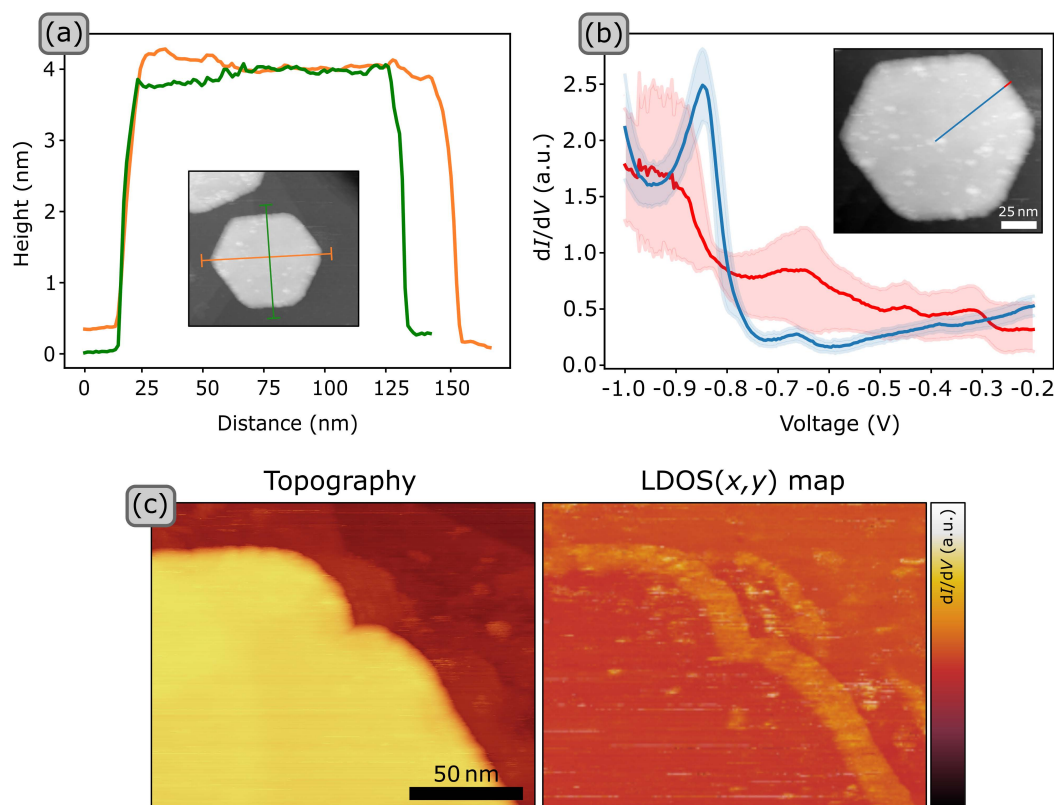


**Figure 3** Characterization of the electronic structure of $Bi_2Se_3$ platelets, 4 QLs in thickness, with scanning tunneling microscopy and spectroscopy. (a) Height determination a platelet on a gold (111) surface by STM topography: the STM height difference of 4 nm shows that the platelet has a uniform thickness of 4 quintuple layers. (b) d$I$/d$V$ spectrum, i.e., LDOS($E$,$x$,$y$). Blue spectrum: LDOS($E$,$x$,$y$) averaged over 25 positions of the blue line (inset) reflecting the density of states of the interior of the platelet. The blue shaded region represents the standard deviation. Red spectrum: the LDOS($E$,$x$,$y$) averaged over 5 positions over the red line (inset) presenting the density of states at the edge. The red shaded region represents the standard deviation. (c) Topographic image and LDOS($x$,$y$) map at the edge of a second platelet of 4 QLs in thickness. For the map, a bias of −0.39 V was used. This map clearly shows the presence of a ~ 10 nm wide state localized at the edge. Images adapted with permission from Ref. [66], © Moes, J. R. et al. 2024. Further permissions related to the material excerpted should be directed to the ACS.

The method to deposit platelets on a gold(111) substrate and prepare the sample for reliable scanning tunneling microscopy and spectroscopy is described elsewhere [66]. Here, we should mention that it is far from trivial to transfer wet-chemically prepared nanocrystals into the ultra-high vacuum of an STM and obtain the standards of surface cleanliness to allow reliable microscopy and spectroscopy [148–150]. The thickness of a given platelet under investigation is measured from the microscopic height difference with the gold substrate, see Fig. 3(a). With cryogenic tunneling spectroscopy, we measured the d$I$/d$V$ vs. $V$ spectrum ($I$ is the tunneling current between tip and sample, $V$ is the bias applied between the tip and the sample), which can be approximated as the local density of electronic states LDOS($E,x,y$) [151]. For each platelet that we investigated, we measured the LDOS($E,x,y$) of the interior and edge regions. Results for two platelets, both with a thickness of 4 QLs, are presented in Fig. 3(b). In the interior of the crystal (blue line in inset, blue spectrum), this platelet shows the same LDOS($E$) as an MBE grown $Bi_2Se_3$ crystal [148–150]. This holds more generally for platelets in the 2–6 QLs thickness region. Below −0.5 V, an increasing LDOS($E$) is observed, reflecting the valence bands at negative bias. Between −0.5 and 0 V, there is a "band-gap" region with low LDOS($E$), followed by a region of increasing LDOS($E$) reflecting the conduction bands. Interestingly, the spectrum changes abruptly when the tip approaches the edge of the nanocrystal at the last 10 nm from the boundary (Fig. 3(b) inset red line, and red d$I$/d$V$ vs. $V$ spectrum). In this edge region of about 10 nm in width, the LDOS($E$) shows a clear relative increase in the band-gap region. Indeed, when the LDOS(x,y) is mapped over the entire crystal at a given voltage in this range, a 10 nm wide edge region with enhanced LDOS($x,y$) emerges, see Figs. 3(c). These data provide a strong indication for the presence of quantum channel at the edge. We reproducibly observed such a channel for nanoplatelets of 4, 5, and 6 QLs in thickness [66], while the channel was absent in platelets of 1, 2 QLs. In the case of platelets consisting of 3 QLs, about half of the platelets showed (weaker) features that may point to the presence of an edge state.

As mentioned previously, helical edge modes in TIs are protected by TRS. Theoretically, a magnetic field applied perpendicular to a $Bi_2Se_3$ platelet breaks TRS, which should then impede the quantum spin Hall effect. However, in other QSHIs, it was found that the edge states only deteriorate at high magnetic fields (> 8 T) [152–156]. Hence, even at magnetic fields up to 10 T, the impact of the combined Zeeman effect and Lorentz force

are too weak to destroy the quantum spin Hall channel at the edge of these materials. For $Bi_2Se_3$ platelets (4–6 QLs), we observed only small quantitative changes in the LDOS($E,x,y$) under a magnetic field up to 5 T [66]. In addition to applying a magnetic field, we investigated what happens to the edge states when magnetic atoms are present on the $Bi_2Se_3$ platelets by depositing Mn ions on the sample. The results are presented in Fig. 4 for platelets of 4 and 5 QLs. In general, we observe that the edge state is spatially less uniform in intensity, with clear intensity modulations (see 4 QL platelets). We tentatively interpret these modulations as being interfering forward and backscattered modes, although the lack of atomic resolution prevents us from proving the presence and position of Mn atoms in an independent way. When twice as much Mn is deposited, the edge state cannot be observed anymore (see 5 QL platelet). The influence of magnetic adatoms is better studied in materials prepared under ultra-high vacuum (e.g. in the STM), where magnetic adatoms can be visualized owing to the atomic resolution. Thus far, this level of control has been rare, although Jäck et al., reported the quasi-particle interference in topological propagating states on a double layer of Bi by a magnetic Fe-cluster [157].

To better understand the nature of the observed edge states, we performed simulations on two levels. An 8-band k·p continuum model provides $Z_2$ invariants showing that two-dimensional $Bi_2Se_3$ with a thickness of 3–5 QLs is a QSHI. The *ab-initio* DFT calculation (with full atomic relaxation) suggests that 2D $Bi_2Se_3$ of 4–6 QLs is non-trivial. This slight difference should not be taken too strictly; the *ab-initio* simulations show that the protecting inverted gap is rather small (about 50 meV), while atomic strain can result in a phase transition from topological to trivial, or the other way around [66]. Furthermore, both models show the existence of helical edge states with spin-momentum locking, with the width of the edge state being about 8 nm, in excellent agreement with the experimental results. In addition, the DFT simulations show that the presence or absence of topological edge states does not depend on the crystallographic termination, while the precise energy-momentum dispersion relation is specific for a given crystallographic termination of the $Bi_2Se_3$ crystal. Further research should focus on the electron–electron interactions in such systems, as this may affect surface or edge conductivity [158, 159].

The results presented in this section serve as an example of how colloidal nanocrystals are useful model systems to investigate topological insulators. The $Sb_2X_3$ and $Bi_2X_3$ families (where X = S, Se, Te), along with compounds having mixed stoichiometry, all
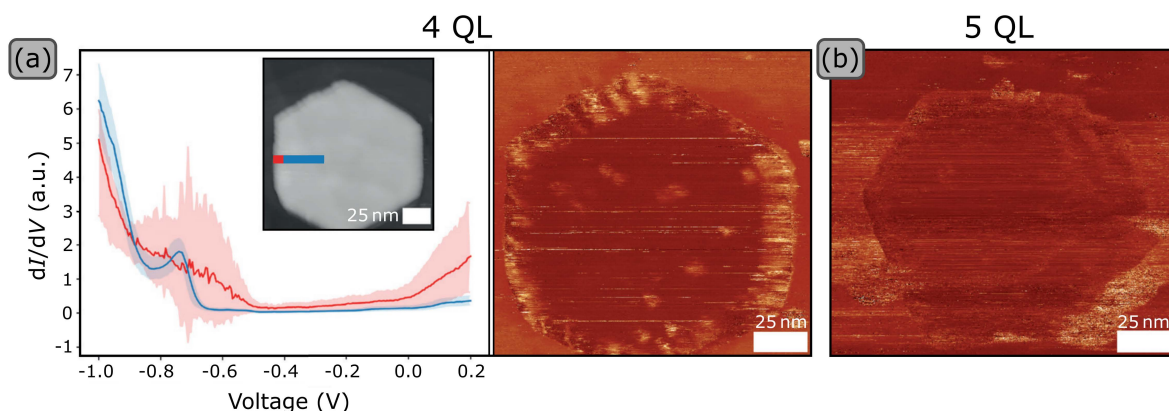


**Figure 4** Effect of magnetic Mn atoms on the edge state observed on $Bi_2Se_3$ platelets of 4 and 5 QLs in thickness. After deposition of the platelets on a gold(111) sample, a dose of Mn atoms was deposited on the sample. Due to the lack of atomic resolution, the Mn atoms are not visible. (a) The density of states LDOS($E,x,y$) measured in the interior of the platelet (blue) at 30 positions over the blue line with the shade as standard deviation, and at the edge (red) measured over 7 positions on the red line, reflecting an edge state in the last 10 nm from the edge. The LDOS($x,y$) map taken at a bias of −0.4 V shows a 10 nm wide edge state with intensity modulations, likely reflecting back-forward mode interference due to scattering of the edge electrons with magnetic Mn. (b) LDOS($x,y$) map taken at a bias of −0.4 V for a 5 QL platelet after a second dose of Mn atoms was deposited on the sample. The edge states appear more heavily deteriorated.
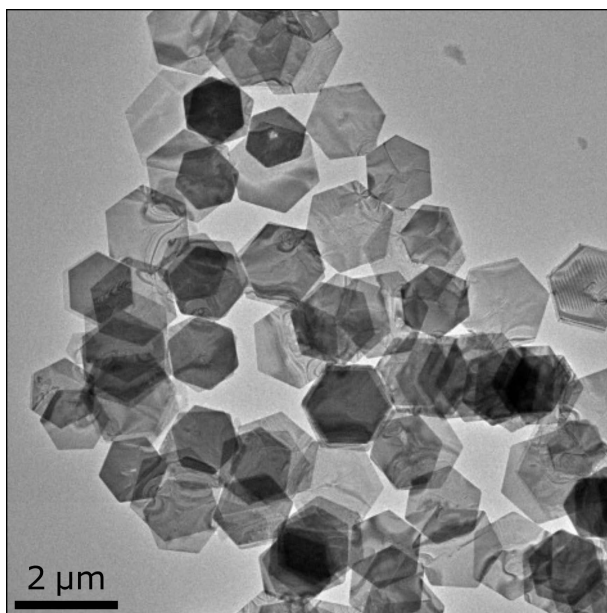
**Figure 5** TEM image of Bi$_2$Te$_3$ nanoplatelets synthesized with a wet-chemical method (as described in Ref. [163]).

share a similar layered (van der Waals) structure and comparable band structures to Bi$_2$Se$_3$ [56]. In the heavier members of these families, such as Bi$_2$Te$_3$ and Sb$_2$Te$_3$, spin-orbit effects induce band inversion and non-trivial topology. Therefore, similar to Bi$_2$Se$_3$, the assets of wet chemical preparation and colloidal science can aid in our understanding of the topological properties in these systems. Appropriate synthesis methods for various compounds have already been reported in the literature [141, 160–163]. For example, in Fig. 5, we show Bi$_2$Te$_3$ nanoplatelets with lateral dimensions in the 1–2 µm range. These platelets can also be used to study the transition from a three-dimensional to a two-dimensional TI. To be able to perform such a study, better control over the thickness of the platelets is required.

# 6 Topological crystalline insulators

As mentioned previously, topological crystalline insulators present a different class of topological materials in which the protected conductive surface states strongly depend on the crystal symmetry. This adds a layer of complexity and richness to their topological classification and opens new avenues for theoretical and experimental research. SnTe is a key example of a TCI [76]. Experimentally, the presence/absence of the Dirac-type states on crystal surfaces has been investigated with ARPES, cryogenic scanning tunneling spectroscopy, Landau level spectroscopy, IR reflection spectroscopy, and transport measurements [89, 164–175]. The signatures of one-dimensional quantum channels have been observed with cryogenic scanning tunneling miscorscopy/spectroscopy [90] and discussed on a theoretical basis [176].

The simple cubic rock-salt lattice of SnTe makes it a cousin to the trivial insulator family of PbX (X = S, Se, Te) nanocrystals, which have been extensively investigated in colloidal nanoscience [177–184]. In such rock-salt crystals, the (100) mixed Metal/X surfaces are the most stable. Hence, the nanocrystals have the propensity to grow in a cubic shape that displays six (100)-type facets, with truncations of the eight edges displaying smaller (110) facets, and at the corner points revealing (111) facets (Metal or X terminated). This is driven by minimizing the overall surface, edge and point energy, although the crystal shape is very sensitive to the ligand chemistry of the nanocrystals [185]. The surface and ligand chemistry has been extensively investigated and fine-tuned for

PbX nanocrystals, both to obtain electronically passivated surfaces and/or use the nanocrystals to form superlattices by assembly and oriented attachment [29, 30, 186–191]. The ionic nature of the PbX family crystals also allows for cationic exchange [192–199]. In this way, new types of nanocrystals and superlattices can be obtained difficult to get by direct synthesis.

From the electronic perspective, the class of SnX and PbX (X = S, Se, Te) materials are also similar. Their small (range 100 meV) fundamental gaps are located at the 4 L-points in the Brillouin zone [73, 76, 180, 181, 200, 201]. Intervalley coupling results in a breaking of the degeneracy of the valence and conduction bands. As the effective carrier mass in both the valence- and conduction bands are small, the effects of particle-wave confinement are considerable and the bands can be shifted from their bulk value to values around 1 eV by reducing the nanocrystal size [177, 202, 203]. Opto-electronic applications include IR detectors, IR lasers and eventually solar cells [204–206].

Despite their structural and electronic similarities, SnTe is a TCI while PbTe and SnSe are trivial insulators [207–209]. The topological properties of SnTe are specifically related to its mirror symmetry. Although this mirror symmetry is a necessary condition, it is clearly not sufficient to induce a band inversion. Based on first-principles calculations, it was found that in PbTe, the conduction and valence bands derive primarily from the p-orbitals of Pb and Te atoms respectively, which characterizes PbTe as a trivial insulator. In SnTe, however, the band structure is inverted at the L points in the Brillouin zone, meaning that the conduction band edge originates from Te, while the valence band edge derives from Sn. This corresponds to an inverted band structure, where the effective mass becomes negative [76]. Interestingly, when going from PbTe to SnTe, Pb$_{1-x}$Sn$_x$Te materials show a trivial-to-TCI phase transition when $x$ is raised above 0.25 [74, 83, 84, 89, 166].

In SnTe, crystal mirror symmetry protects the surface states on surfaces that are symmetric about the {110} mirror planes, e.g. planes with Miller indices {hhk}. Figure 6(a) shows an atomic schematic of the rock-salt lattice (as e.g. found for of PbSe nanocrystals [185]) with indication of the (100) (110) and (111) facets, and a mirror plane along the [110] direction drawn in the (100) plane. For rock-salt crystals, the {100} family of planes have the lowest surface energy and are thus likely to be dominant at the surface [210]. Figure 6(b) shows how the topological properties of SnTe are related to its structural symmetries on the {100} surface. The image shows the truncated octahedron Brillouin zone, with L points at the center of each hexagonal face and X points at the center of each square face. The Γ point is indicated with a star. By projecting the L-points on the (100) family of lattice planes, indicated with arrows, two *L* points are projected to the same momentum point $\overline{X}_1$ or $\overline{X}_2$. This results in an interaction that creates a pair of Dirac cones shifted slightly away from $\overline{X}$ to create different types of topological surface states with an unusual band dispersion and spin texture [76, 81, 83, 84]. For the (111) surface, the L points all project onto a different momentum, and thus do not interact.

In contrast to topology induced by spin-orbit coupling, where a bulk-boundary connection results in a Dirac state at the surface or edge independent of the atomic configuration, in TCIs the atomic symmetry at the surfaces is critical for the observation of non-trivial topology [80, 208, 209]. For instance, it becomes clear from Fig. 6(a) that the mirror symmetry at the (100) rock-salt surface breaks down for specific atomic distortions, an effect which may result in an inverse TCI → trivial transition [79]. We note that random atomic displacements can be considered as averaged disorder, which does not break mirror symmetry. However, the precise atomic registry of the displayed surfaces, sometimes
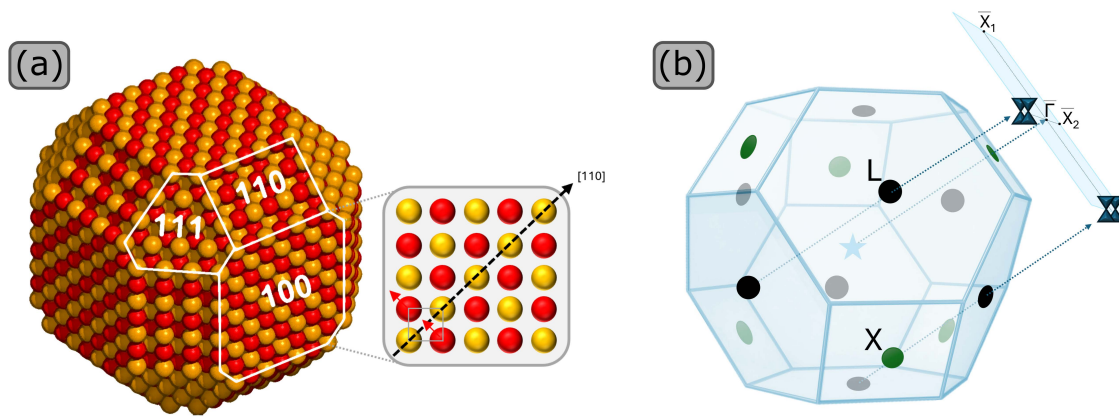
**Figure 6** Rock-salt lattice with sigh-symmetry surfaces frequently observed in crystalline topological crystalline insulators such as SnTe. (a) Model of a (nano)crystal with the most stable (lowest energy) family of (100) planes. Truncations of the edges result in the (110) family of planes, while truncation of the corners result in higher-energy (111) planes. In colloidal nanocrystals, the higher-energy facets are strongly coordinated by organic ligands, atomic distortion can lower the symmetry of these surfaces. The schematic in grey shows a (100) plane with a dashed mirror symmetry line. Atomic distortions at the surface (red arrows) can break the mirror symmetry in the plane. (b) Face-centered-cubic Brillouin zone inspired by Ref. [76], © Springer Nature Limited 2012. The L points are given in black, the X points in green, and the Γ point is indicated with a star. The projection of the L points onto the (100) surface is shown with blue arrows, yielding four Dirac points located on the four equivalent $\overline{\Gamma}-\overline{X}$ lines (only visualized for two cases due to symmetry).
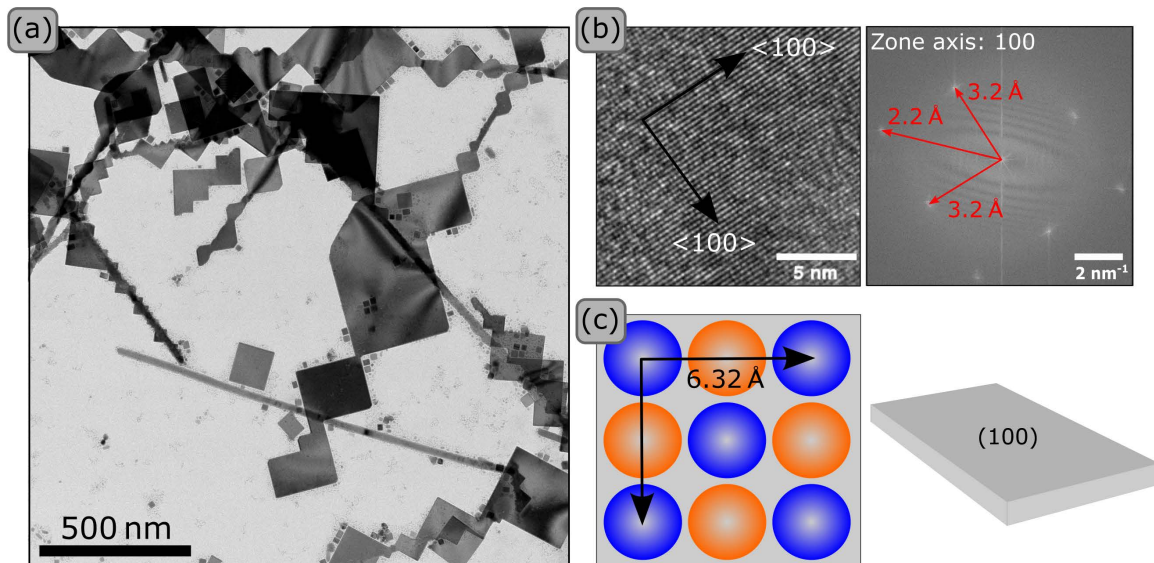


**Figure 7** Wet chemical synthesis of flat SnTe nanosheets. (a) Transmission electron microscopy (TEM) image of SnTe sheets of about 10–100 nm in thickness. The crystal shape points to the top and bottom being (100) type of surfaces of the rock-salt lattice. (b) High resolution TEM image showing the atomic rows in the <100> viewing direction, with a 0.32 nm distance between the atom columns (derived from the FFT), confirming that this is the (100) family. The schematic in (c) shows the orientation and crystal structure of the synthesized sheets.

affected by (ligand) surface chemistry, is critical [211]. For the TCI SnTe, this has resulted in crystal shape and surface engineering with the aim to form anisotropic wires, ribbons and plates that display microsized (001) surfaces with protected Dirac-type surface states [167, 208, 209, 212–216]. As an example, we show SnTe crystals that have been prepared by wet-chemical synthesis (the synthesis method will be detailed elsewhere). Figure 7(a) shows, besides a small amount of small cubic crystals, large crystalline SnTe sheets. The high resolution TEM image and corresponding Fast Fourier Transform (FFT) in Fig. 7(b) show that the top and bottom surface are (100) terminated (shown in Fig. 7(c)), and should therefore display Dirac-type surface states if the surface is not distorted. It will be of strong interest to investigate these surface states and their dependence on the structural symmetries and sheet thickness. If the sheets can be prepared thin enough, will this induce a gapped surface state,

resulting in a two-dimensional TCI with one dimensional quantum states at the edge? Considering the proof-of-concept experiments involving $Bi_2Se_3$ described above, a strong chemical expertise may certainly aid in exploring this hypothesis. The preparation of mixed $Pb_xSn_{1-x}Te/Se$ crystals by cation exchange or one-pot colloidal synthesis routes also presents an interesting approach for the exploration of the trivial to nontrivial phase transition in TCIs [217, 218].

## 7   What is next?

Despite being over a decade old, the field of topological insulators is still in its infancy, especially with respect to practical applications. In this review, we have highlighted how colloidal nanocrystals could advance the field from a fundamental perspective. We also note that the flexibility of colloidal synthesis

procedures allows unparalleled freedom of material design. The processability of colloidal nanocrystals may therefore be of use for device fabrication. Although current material design and device fabrication mainly revolves around thin film growth techniques, nanocrystals are also emerging as promising candidates for applications such as thermoelectric devices [219].

Finally, we wish to emphasize that to address the challenges outlined in this review and to solve upcoming issues in device design, an interdisciplinary approach will be required. Over four decades of rigorous research in colloidal science has resulted in considerable control over crystal dimensions, surface properties, nanocrystal assembly and spatially-resolved deposition; expertise from which the field of topological materials could benefit. With chemists guiding material design and optimization, physicists providing insights into the origin of topological effects, and materials scientists bridging the gap between fundamental studies and practical applications, significant advancements can be made in the field of quantum materials.

## Acknowledgements

## References

[1] Murray, C. B.; Norris, D. J.; Bawendi, M. G. Synthesis and characterization of nearly monodisperse CdE (E = sulfur, selenium, tellurium) semiconductor nanocrystallites. *J. Am. Chem. Soc.* **1993**, *115*, 8706–8715.

[2] Alivisatos, A. P. Semiconductor clusters, nanocrystals, and quantum dots. *Science,* **1996**, *271*, 933–937.

[3] Coe, S.; Woo, W. K.; Bawendi, M.; Bulović, V. Electroluminescence from single monolayers of nanocrystals in molecular organic devices. *Nature,* **2002**, *420*, 800–803.

[4] Schlamp, M. C.; Peng, X. G.; Alivisatos, A. P. Improved efficiencies in light emitting diodes made with CdSe(CdS) core/shell type nanocrystals and a semiconducting polymer. *J. Appl. Phys.* **1997**, *82*, 5837–5842.

[5] Mashford, B. S.; Stevenson, M.; Popovic, Z.; Hamilton, C.; Zhou, Z. Q.; Breen, C.; Steckel, J.; Bulovic, V.; Bawendi, M.; Coe-Sullivan, S. et al. High-efficiency quantum-dot light-emitting devices with enhanced charge injection. *Nat. Photon.* **2013**, *7*, 407–412.

[6] Chen, O.; Wei, H.; Maurice, A.; Bawendi, M.; Reiss, P. Pure colors from core-shell quantum dots. *MRS Bull.* **2013**, *38*, 696–702.

[7] Kovalenko, M. V.; Manna, L.; Cabot, A.; Hens, Z.; Talapin, D. V.; Kagan, C. R.; Klimov, V. I.; Rogach, A. L.; Reiss, P.; Milliron, D. J. et al. Prospects of nanoscience with nanocrystals. *ACS Nano* **2015**, *9*, 1012–1057.

[8] Prins, P. T.; Alimoradi Jazi, M.; Killilea, N. A.; Evers, W. H.; Geiregat, P.; Heiss, W.; Houtepen, A. J.; Delerue, C.; Hens, Z.; Vanmaekelbergh, D. The fine-structure constant as a ruler for the band-edge light absorption strength of bulk and quantum-confined semiconductors. *Nano Lett.* **2021**, *21*, 9426–9432.

[9] Wagner, A. M.; Knipe, J. M.; Orive, G.; Peppas, N. A. Quantum dots in biomedical applications. *Acta Biomater.* **2019**, *94*, 44–63.

[10] Heiner Linke, T. N. C. f. C. Quantum dots, seeds of Nanoscience. *Nobel Prize Chemistry, Motivation* **2023**.

[11] Norris, D. J.; Nirmal, M.; Murray, C. B.; Sacra, A.; Bawendi, M. G. Size dependent optical spectroscopy of II-VI semiconductor nanocrystallites (quantum dots). *Z. Phys. D Atoms, Molec. Clusters* **1993**, *26*, 355–357.

[12] Tamm, I. E. A possible kind of electron binding on crystal surfaces. *Z. Phys*. **1932**, *76*.

[13] Shockley, W. On the surface states associated with a periodic potential. *Phys. Rev.* **1939**, *56*, 317–323.

[14] Houtepen, A. J.; Hens, Z.; Owen, J. S.; Infante, I. On the origin of surface traps in colloidal II-VI semiconductor nanocrystals. *Chem. Mater.* **2017**, *29*, 752–761.

[15] Kuno, M.; Lee, J. K.; Dabbousi, B. O.; Mikulec, F. V.; Bawendi, M. G. The band edge luminescence of surface modified CdSe nanocrystallites: Probing the luminescing state. *J. Chem. Phys.* **1997**, *106*, 9869–9882.

[16] Moreels, I.; Fritzinger, B.; Martins, J. C.; Hens, Z. Surface chemistry of colloidal PbSe nanocrystals. *J. Am. Chem. Soc.* **2008**, *130*, 15081–15086.

[17] Kovalenko, M. V.; Scheele, M.; Talapin, D. V. Colloidal nanocrystals with molecular metal chalcogenide surface ligands. *Science* **2009**, *324*, 1417–1420.

[18] Nag, A.; Kovalenko, M. V.; Lee, J. S.; Liu, W. Y.; Spokoyny, B.; Talapin, D. V. Metal-free inorganic ligands for colloidal nanocrystals: S²⁻, HS⁻, Se²⁻, HSe⁻, Te²⁻, HTe⁻, TeS₃²⁻, OH⁻, and NH₂⁻ as surface ligands. *J. Am. Chem. Soc.* **2011**, *133*, 10612–10620.

[19] Ithurria, S.; Talapin, D. V. Colloidal atomic layer deposition (c-ALD) using self-limiting reactions at nanocrystal surface coupled to phase transfer between polar and nonpolar media. *J. Am. Chem. Soc.* **2012**, *134*, 18585–18590.

[20] Moreels, I.; Justo, Y.; De Geyter, B.; Haustraete, K.; Martins, J. C.; Hens, Z. Size-tunable, bright, and stable PbS quantum dots: A surface chemistry study. *ACS Nano* **2011**, *5*, 2004–2012.

[21] Boles, M. A.; Ling, D. S.; Hyeon, T.; Talapin, D. V. The surface science of nanocrystals. *Nat. Mater.* **2016**, *15*, 141–153.

[22] Hines, M. A.; Guyot-Sionnest, P. Synthesis and characterization of strongly luminescing ZnS-capped CdSe nanocrystals. *J. Phys. Chem.* **1996**, *100*, 468–471.

[23] Dabbousi, B. O.; Rodriguez-Viejo, J.; Mikulec, F. V.; Heine, J. R.; Mattoussi, H.; Ober, R.; Jensen, K. F.; Bawendi, M. G. (CdSe)ZnS core-shell quantum dots: Synthesis and characterization of a size series of highly luminescent nanocrystallites. *J. Phys. Chem. B* **1997**, *101*, 9463–9475.

[24] Peng, X. G.; Schlamp, M. C.; Kadavanich, A. V.; Alivisatos, A. P. Epitaxial growth of highly luminescent CdSe/CdS core/shell nanocrystals with photostability and electronic accessibility. *J. Am. Chem. Soc.* **1997**, *119*, 7019–7029.

[25] Talapin, D. V.; Mekis, I.; Götzinger, S.; Kornowski, A.; Benson, O.; Weller, H. CdSe/CdS/ZnS and CdSe/ZnSe/ZnS core–shell–shell nanocrystals. *J. Phys. Chem. B* **2004**, *108*, 18826–18831.

[26] Murray, C. B.; Kagan, C. R.; Bawendi, M. G. Self-organization of CdSe nanocrystallites into three-dimensional quantum dot superlattices. *Science* **1995**, *270*, 1335–1338.

[27] Dong, A. G.; Chen, J.; Vora, P. M.; Kikkawa, J. M.; Murray, C. B. Binary nanocrystal superlattice membranes self-assembled at the liquid–air interface. *Nature* **2010**, *466*, 474–477.

[28] Evers, W. H.; De Nijs, B.; Filion, L.; Castillo, S.; Dijkstra, M.;

Vanmaekelbergh, D. Entropy-driven formation of binary semiconductor-nanocrystal superlattices. *Nano Lett.* 2010, *10*, 4235–4241.

[29] Boneschanscher, M. P.; Evers, W. H.; Geuchies, J. J.; Altantzis, T.; Goris, B.; Rabouw, F. T.; Van Rossum, S. A. P.; Van Der Zant, H. S. J.; Siebbeles, L. D. A.; Van Tendeloo, G. et al. Long-range orientation and atomic attachment of nanocrystals in 2D honeycomb superlattices. *Science* 2014, *344*, 1377–1380.

[30] Geuchies, J. J.; Van Overbeek, C.; Evers, W. H.; Goris, B.; De Backer, A.; Gantapara, A. P.; Rabouw, F. T.; Hilhorst, J.; Peters, J. L.; Konovalov, O. et al. *In situ* study of the formation mechanism of two-dimensional superlattices from PbSe nanocrystals. *Nat. Mater.* 2016, *15*, 1248–1254.

[31] Ithurria, S.; Dubertret, B. Quasi 2D colloidal CdSe platelets with thicknesses controlled at the atomic level. *J. Am. Chem. Soc.* 2008, *130*, 16504–16505.

[32] Manna, L.; Scher, E. C.; Alivisatos, A. P. Synthesis of soluble and processable rod-, arrow-, teardrop-, and tetrapod-shaped CdSe nanocrystals. *J. Am. Chem. Soc.* 2000, *122*, 12700–12706.

[33] Fedin, I.; Talapin, D. V. Colloidal CdSe quantum rings. *J. Am. Chem. Soc.* 2016, *138*, 9771–9774.

[34] Salzmann, B. B. V.; Vliem, J. F.; Maaskant, D. N.; Post, L. C.; Li, C.; Bals, S.; Vanmaekelbergh, D. From CdSe nanoplatelets to quantum rings by thermochemical edge reconfiguration. *Chem. Mater.* 2021, *33*, 6853–6859.

[35] Dubois, F.; Mahler, B.; Dubertret, B.; Doris, E.; Mioskowski, C. A versatile strategy for quantum dot ligand exchange. *J. Am. Chem. Soc.* 2007, *129*, 482–483.

[36] Dong, A. G.; Ye, X. C.; Chen, J.; Kang, Y. J.; Gordon, T.; Kikkawa, J. M.; Murray, C. B. A generalized ligand-exchange strategy enabling sequential surface functionalization of colloidal nanocrystals. *J. Am. Chem. Soc.* 2011, *133*, 998–1006.

[37] Xie, R. G.; Battaglia, D.; Peng, X. G. Colloidal InP nanocrystals as efficient emitters covering blue to near-infrared. *J. Am. Chem. Soc.* 2007, *129*, 15432–15433.

[38] Tessier, M. D.; Dupont, D.; De Nolf, K.; De Roo, J.; Hens, Z. Economic and size-tunable synthesis of InP/ZnE (E = S, Se) colloidal quantum dots. *Chem. Mater.* 2015, *27*, 4893–4898.

[39] Van Der Stam, W.; Berends, A. C.; Rabouw, F. T.; Willhammar, T.; Ke, X. X.; Meeldijk, J. D.; Bals, S.; De Mello Donega, C. Luminescent $CuInS_2$ quantum dots by partial cation exchange in $Cu_{2-x}S$ nanocrystals. *Chem. Mater.* 2015, *27*, 621–628.

[40] Chang, C. C.; Chen, J. K.; Chen, C. P.; Yang, C. H.; Chang, J. Y. Synthesis of eco-friendly $CuInS_2$ quantum dot-sensitized solar cells by a combined *ex situ/in situ* growth approach. *ACS Appl. Mater. Interfaces* 2013, *5*, 11296–11306.

[41] Giansante, C.; Infante, I. Surface traps in colloidal quantum dots: A combined experimental and theoretical perspective. *J. Phys. Chem. Lett.* 2017, *8*, 5209–5215.

[42] Giansante, C.; Infante, I.; Fabiano, E.; Grisorio, R.; Suranna, G. P.; Gigli, G. "Darker-than-Black" PbS quantum dots: Enhancing optical absorption of colloidal semiconductor nanocrystals via short conjugated ligands. *J. Am. Chem. Soc.* 2015, *137*, 1875–1886.

[43] Kirkwood, N.; Monchen, J. O. V.; Crisp, R. W.; Grimaldi, G.; Bergstein, H. A. C.; Du Fossé, I.; Van Der Stam, W.; Infante, I.; Houtepen, A. J. Finding and fixing traps in II-VI and III-V colloidal quantum dots: The importance of Z-type ligand passivation. *J. Am. Chem. Soc.* 2018, *140*, 15712–15723.

[44] Xiao, P. W.; Zhang, Z. F.; Ge, J. J.; Deng, Y. L.; Chen, X. F.; Zhang, J.-R.; Deng, Z. T.; Kambe, Y.; Talapin, D. V.; Wang, Y. Y. Surface passivation of intensely luminescent all-inorganic nanocrystals and their direct optical patterning. *Nat. Commun.* 2023, *14*, 49.

[45] Bodnarchuk, M. I.; Boehme, S. C.; Ten Brinck, S.; Bernasconi, C.; Shynkarenko, Y.; Krieg, F.; Widmer, R.; Aeschlimann, B.; Günther, D.; Kovalenko, M. V. et al. Rationalizing and controlling the surface structure and electronic passivation of cesium lead halide nanocrystals. *ACS Energy Lett.* 2019, *4*, 63–74.

[46] Qi, X. L.; Zhang, S. C. The quantum spin Hall effect and topological insulators. *Phys. Today* 2010, *63*, 33–38.

[47] Murakami, S. Quantum spin Hall systems and topological insulators. *New J. Phys.* 2011, *13*, 105007.

[48] Lee, S. S.; Ryu, S. Many-body generalization of the $Z_2$ topological invariant for the quantum spin Hall effect. *Phys. Rev. Lett.* 2008, *100*, 186807.

[49] Raghu, S.; Qi, X. L.; Honerkamp, C.; Zhang, S. C. Topological Mott insulators. *Phys. Rev. Lett.* 2008, *100*, 156401.

[50] Hasan, M. Z.; Kane, C. L. *Colloquium*: Topological insulators. *Rev. Mod. Phys.* 2010, *82*, 3045–3067.

[51] Moore, J. E. The birth of topological insulators. *Nature* 2010, *464*, 194–198.

[52] Felser, C.; Qi, X. L. Topological insulators. *MRS Bull.* 2014, *39*, 843–846.

[53] Dolcetto, G.; Sassetti, M.; Schmidt, T. L. Edge physics in two-dimensional topological insulators. *La Rivista del Nuovo Cimento* 2016, *39*, 113–154.

[54] Rachel, S. Interacting topological insulators: A review. *Rep. Prog. Phys.* 2018, *81*, 116501.

[55] Bradlyn, B.; Elcoro, L.; Cano, J.; Vergniory, M. G.; Wang, Z. J.; Felser, C.; Aroyo, M. I.; Bernevig, B. A. Topological quantum chemistry. *Nature* 2017, *547*, 298–305.

[56] Zhang, H. J.; Liu, C. X.; Qi, X. L.; Dai, X.; Fang, Z.; Zhang, S. C. Topological insulators in $Bi_2Se_3$, $Bi_2Te_3$ and $Sb_2Te_3$ with a single Dirac cone on the surface. *Nat. Phys.* 2009, *5*, 438–442.

[57] Fu, L.; Kane, C. L.; Mele, E. J. Topological insulators in three dimensions. *Phys. Rev. Lett.* 2007, *98*, 106803.

[58] Bernevig, B. A.; Hughes, T. L.; Zhang, S. C. Quantum spin Hall effect and topological phase transition in HgTe quantum wells. *Science* 2006, *314*, 1757–1761.

[59] Hsieh, D.; Qian, D.; Wray, L.; Xia, Y.; Hor, Y. S.; Cava, R. J.; Hasan, M. Z. A topological Dirac insulator in a quantum spin Hall phase. *Nature* 2008, *452*, 970–974.

[60] Hor, Y. S.; Richardella, A.; Roushan, P.; Xia, Y.; Checkelsky, J. G.; Yazdani, A.; Hasan, M. Z.; Ong, N. P.; Cava, R. J. p-type $Bi_2Se_3$ for topological insulator and low-temperature thermoelectric applications. *Phys. Rev. B: Condens. Matter Mater. Phys.* 2009, *79*, 195208.

[61] Roy, R. Topological phases and the quantum spin Hall effect in three dimensions. *Phys. Rev. B: Condens. Matter Mater. Phys.* 2009, *79*, 195322.

[62] Moore, J. E.; Balents, L. Topological invariants of time-reversal-invariant band structures. *Phys. Rev. B: Condens. Matter Mater. Phys.* 2007, *75*, 121306.

[63] Kane, C. L.; Mele, E. J. Quantum spin Hall effect in graphene. *Phys. Rev. Lett.* 2005, *95*, 226801.

[64] Kane, C. L.; Mele, E. J. $Z_2$ topological order and the quantum spin Hall effect. *Phys. Rev. Lett.* 2005, *95*, 146802.

[65] Zhang, F.; Kane, C. L.; Mele, E. J. Surface states of topological insulators. *Phys. Rev. B: Condens. Matter Mater. Phys.* 2012, *86*, 081303.

[66] Moes, J. R.; Vliem, J. F.; De Melo, P. M. M. C.; Wigmans, T. C.; Botello-Méndez, A. R.; Mendes, R. G.; Van Brenk, E. F.; Swart, I.; Maisel Licerán, L.; Stoof, H. T. C. et al. Characterization of the edge states in colloidal $Bi_2Se_3$ platelets. *Nano Lett.* 2024, *24*, 5110–5116.

[67] Avron, J. E.; Osadchy, D.; Seiler, R. A topological look at the quantum Hall effect. *Phys. Today* 2003, *56*, 38–42.

[68] Klitzing, K. v.; Chakraborty, T.; Kim, P.; Madhavan, V.; Dai, X.; McIver, J.; Tokura, Y.; Savary, L.; Smirnova, D.; Rey, A. M. et al. 40 years of the quantum Hall effect. *Nat. Rev. Phys.* 2020, *2*, 397–401.

[69] Keimer, B.; Moore, J. E. The physics of quantum materials. *Nat. Phys.* 2017, *13*, 1045–1055.

[70] Konig, M.; Wiedmann, S.; Brune, C.; Roth, A.; Buhmann, H.; Molenkamp, L. W.; Qi, X. L.; Zhang, S. C. Quantum spin Hall insulator state in HgTe quantum wells. *Science* 2007, *318*, 766–770.

[71] Brüne, C.; Liu, C. X.; Novik, E. G.; Hankiewicz, E. M.; Buhmann, H.; Chen, Y. L.; Qi, X. L.; Shen, Z. X.; Zhang, S. C.; Molenkamp, L. W. Quantum Hall effect from the topological surface states of strained bulk HgTe. *Phys. Rev. Lett.* 2011, *106*, 126803.

[72] Fu, L. Topological crystalline insulators. *Phys. Rev. Lett.* **2011**, *106*, 106802.

[73] Ando, Y.; Fu, L. Topological crystalline insulators and topological superconductors: From concepts to materials. *Annu. Rev. Condens. Matter Phys.* **2015**, *6*, 361–381.

[74] Ozawa, H.; Yamakage, A.; Sato, M.; Tanaka, Y. Topological phase transition in a topological crystalline insulator induced by finite-size effects. *Phys. Rev. B* **2014**, *90*, 045309.

[75] Isobe, H.; Fu, L. Theory of interacting topological crystalline insulators. *Phys. Rev. B* **2015**, *92*, 081304.

[76] Hsieh, T. H.; Lin, H.; Liu, J. W.; Duan, W. H.; Bansil, A.; Fu, L. Topological crystalline insulators in the SnTe material class. *Nat. Commun.* **2012**, *3*, 982.

[77] Freeney, S. E.; Van Den Broeke, J. J.; Harsveld Van Der Veen, A. J. J.; Swart, I.; Morais Smith, C. Edge-dependent topology in Kekulé lattices. *Phys. Rev. Lett.* **2020**, *124*, 236404.

[78] Safaei, S.; Galicka, M.; Kacman, P.; Buczko, R. Quantum spin Hall effect in IV-VI topological crystalline insulators. *New J. Phys.* **2015**, *17*, 063041.

[79] Zeljkovic, I.; Okada, Y.; Serbyn, M.; Sankar, R.; Walkup, D.; Zhou, W. W.; Liu, J. W.; Chang, G. Q.; Wang, Y. J.; Hasan, M. Z. et al. Dirac mass generation from crystal symmetry breaking on the surfaces of topological crystalline insulators. *Nat. Mater.* **2015**, *14*, 318–324.

[80] Eremeev, S. V.; Koroteev, Y. M.; Nechaev, I. A.; Chulkov, E. V. Role of surface passivation in the formation of Dirac states at polar surfaces of topological crystalline insulators: The case of SnTe(111). *Phys. Rev. B* **2014**, *89*, 165424.

[81] Tanaka, Y.; Ren, Z.; Sato, T.; Nakayama, K.; Souma, S.; Takahashi, T.; Segawa, K.; Ando, Y. Experimental realization of a topological crystalline insulator in SnTe. *Nat. Phys.* **2012**, *8*, 800–803.

[82] Tanaka, Y.; Shoman, T.; Nakayama, K.; Souma, S.; Sato, T.; Takahashi, T.; Novak, M.; Segawa, K.; Ando, Y. Two types of Dirac-cone surface states on the (111) surface of the topological crystalline insulator SnTe. *Phys. Rev. B* **2013**, *88*, 235126.

[83] Dziawa, P.; Kowalski, B. J.; Dybko, K.; Buczko, R.; Szczerbakow, A.; Szot, M.; Łusakowska, E.; Balasubramanian, T.; Wojek, B. M.; Berntsen, M. H. et al. Topological crystalline insulator states in Pb$_{1-x}$Sn$_x$Se. *Nat. Mater.* **2012**, *11*, 1023–1027.

[84] Xu, S. Y.; Liu, C.; Alidoust, N.; Neupane, M.; Qian, D.; Belopolski, I.; Denlinger, J. D.; Wang, Y. J.; Lin, H.; Wray, L. A. et al. Observation of a topological crystalline insulator phase and topological phase transition in Pb$_{1-x}$Sn$_x$Te. *Nat. Commun.* **2012**, *3*, 1192.

[85] Liu, J. W.; Hsieh, T. H.; Wei, P.; Duan, W. H.; Moodera, J.; Fu, L. Spin-filtered edge states with an electrically tunable gap in a two-dimensional topological crystalline insulator. *Nat. Mater.* **2014**, *13*, 178–183.

[86] Tanaka, Y.; Sato, T.; Nakayama, K.; Souma, S.; Takahashi, T.; Ren, Z.; Novak, M.; Segawa, K.; Ando, Y. Tunability of the *k*-space location of the Dirac cones in the topological crystalline insulator Pb$_{1-x}$Sn$_x$Te. *Phys. Rev. B: Condens. Matter Mater. Phys.* **2013**, *87*, 155105.

[87] Polley, C. M.; Dziawa, P.; Reszka, A.; Szczerbakow, A.; Minikayev, R.; Domagala, J. Z.; Safaei, S.; Kacman, P.; Buczko, R.; Adell, J. et al. Observation of topological crystalline insulator surface states on (111)-oriented Pb$_{1-x}$Sn$_x$Se films. *Phys. Rev. B* **2014**, *89*, 075317.

[88] Tikuišis, K. K.; Wyzula, J.; Ohnoutek, L.; Cejpek, P.; Uhlířová, K.; Hakl, M.; Faugeras, C.; Výborný, K.; Ishida, A.; Veis, M. et al. Landau level spectroscopy of the PbSnSe topological crystalline insulator. *Phys. Rev. B* **2021**, *103*, 155304.

[89] Wojek, B. M.; Dziawa, P.; Kowalski, B. J.; Szczerbakow, A.; Black-Schaffer, A. M.; Berntsen, M. H.; Balasubramanian, T.; Story, T.; Tjernberg, O. Band inversion and the topological phase transition in (Pb, Sn) Se. *Phys. Rev. B* **2014**, *90*, 161202.

[90] Sessi, P.; Di Sante, D.; Szczerbakow, A.; Glott, F.; Wilfert, S.; Schmidt, H.; Bathon, T.; Dziawa, P.; Greiter, M.; Neupert, T. et al. Robust spin-polarized midgap states at step edges of topological crystalline insulators. *Science* **2016**, *354*, 1269–1273.

[91] Rogacheva, E. I.; Nikolaenko, G. O.; Nashchekina, O. N. Transport and thermoelectric properties of the Pb$_{1-x}$Sn$_x$Te topological crystalline insulator in the vicinity of the band inversion. *J. Phys. Chem. Solids* **2023**, *183*, 111635.

[92] Gilbert, M. J. Topological electronics. *Commun. Phys.* **2021**, *4*, 70.

[93] Butch, N. P.; Kirshenbaum, K.; Syers, P.; Sushkov, A. B.; Jenkins, G. S.; Drew, H. D.; Paglione, J. Strong surface scattering in ultrahigh-mobility Bi$_2$Se$_3$ topological insulator crystals. *Phys. Rev. B: Condens. Matter Mater. Phys.* **2010**, *81*, 241301.

[94] Bauer, C.; Lesyuk, R.; Khoshkhoo, M. S.; Klinke, C.; Lesnyak, V.; Eychmüller, A. Surface defines the properties: Colloidal Bi$_2$Se$_3$ nanosheets with high electrical conductivity. *J. Phys. Chem. C* **2021**, *125*, 6442–6448.

[95] Veyrat, L.; Iacovella, F.; Dufouleur, J.; Nowka, C.; Funke, H.; Yang, M.; Escoffier, W.; Goiran, M.; Eichler, B.; Schmidt, O. G. et al. Band bending inversion in Bi$_2$Se$_3$ nanostructures. *Nano Lett.* **2015**, *15*, 7503–7507.

[96] Navrátil, J.; Horák, J.; Plecháček, T.; Kamba, S.; Lošt'ák, P.; Dyck, J. S.; Chen, W.; Uher, C. Conduction band splitting and transport properties of Bi$_2$Se$_3$. *J. Solid State Chem.* **2004**, *177*, 1704–1712.

[97] Peng, H. L.; Lai, K. J.; Kong, D. S.; Meister, S.; Chen, Y. L.; Qi, X. L.; Zhang, S. C.; Shen, Z. X.; Cui, Y. Aharonov-Bohm interference in topological insulator nanoribbons. *Nat. Mater.* **2010**, *9*, 225–229.

[98] Walsh, L. A.; Green, A. J.; Addou, R.; Nolting, W.; Cormier, C. R.; Barton, A. T.; Mowll, T. R.; Yue, R. Y.; Lu, N.; Kim, J. et al. Fermi level manipulation through native doping in the topological insulator Bi$_2$Se$_3$. *ACS Nano* **2018**, *12*, 6310–6318.

[99] Musah, J. D.; Linlin, L.; Guo, C.; Novitskii, A.; Ilyas, A. O.; Serhiienko, I.; Khovaylo, V.; Roy, V. A. L.; Lawrence Wu, C. M. Enhanced thermoelectric performance of bulk bismuth selenide: Synergistic effect of indium and antimony co-doping. *ACS Sustain. Chem. Eng.* **2022**, *10*, 3862–3871.

[100] Steinberg, H.; Gardner, D. R.; Lee, Y. S.; Jarillo-Herrero, P. Surface state transport and ambipolar electric field effect in Bi$_2$Se$_3$ nanodevices. *Nano Lett.* **2010**, *10*, 5032–5036.

[101] Xiu, F.; He, L.; Wang, Y.; Cheng, L. N.; Chang, L. T.; Lang, M. R.; Huang, G.; Kou, X. F.; Zhou, Y.; Jiang, X. W. et al. Manipulating surface states in topological insulator nanoribbons. *Nat. Nanotech.* **2011**, *6*, 216–221.

[102] Kim, D.; Cho, S.; Butch, N. P.; Syers, P.; Kirshenbaum, K.; Adam, S.; Paglione, J.; Fuhrer, M. S. Surface conduction of topological Dirac electrons in bulk insulating Bi$_2$Se$_3$. *Nat. Phys.* **2012**, *8*, 459–463.

[103] Hong, S. S.; Cha, J. J.; Kong, D. S.; Cui, Y. Ultra-low carrier concentration and surface-dominant transport in antimony-doped Bi$_2$Se$_3$ topological insulator nanoribbons. *Nat. Commun.* **2012**, *3*, 757.

[104] Maassen, J.; Lundstrom, M. A computational study of the thermoelectric performance of ultrathin Bi$_2$Te$_3$ films. *Appl. Phys. Lett.* **2013**, *102*, 093103.

[105] Kim, D.; Syers, P.; Butch, N. P.; Paglione, J.; Fuhrer, M. S. Ambipolar surface state thermoelectric power of topological insulator Bi$_2$Se$_3$. *Nano Lett.* **2014**, *14*, 1701–1706.

[106] Liang, J. H.; Cheng, L.; Zhang, J.; Liu, H. J.; Zhang, Z. Y. Maximizing the thermoelectric performance of topological insulator Bi$_2$Te$_3$ films in the few-quintuple layer regime. *Nanoscale* **2016**, *8*, 8855–8862.

[107] He, J.; Tritt, T. M. Advances in thermoelectric materials research: Looking back and moving forward. *Science* **2017**, *357*, eaak9997.

[108] Zhang, J. S.; Feng, X.; Xu, Y.; Guo, M. H.; Zhang, Z. C.; Ou, Y. B.; Feng, Y.; Li, K.; Zhang, H. J.; Wang, L. L. et al. Disentangling the magnetoelectric and thermoelectric transport in topological insulator thin films. *Phys. Rev. B* **2015**, *91*, 075431.

[109] Xu, Y.; Gan, Z. X.; Zhang, S. C. Enhanced thermoelectric performance and anomalous Seebeck effects in topological insulators. *Phys. Rev. Lett.* **2014**, *112*, 226801.

[110] Bauer, C.; Veremchuk, I.; Kunze, C.; Benad, A.; Dzhagan, V. M.; Haubold, D.; Pohl, D.; Schierning, G.; Nielsch, K.; Lesnyak, V. et al. Heterostructured bismuth telluride selenide nanosheets for enhanced thermoelectric performance. *Small Sci.* **2021**, *1*, 2000021.

[111] Venkatasubramanian, R.; Siivola, E.; Colpitts, T.; O'Quinn, B. Thin-

film thermoelectric devices with high room-temperature figures of merit. *Nature* **2001**, *413*, 597–602.

[112] Poudel, B.; Hao, Q.; Ma, Y.; Lan, Y. C.; Minnich, A.; Yu, B.; Yan, X.; Wang, D. Z.; Muto, A.; Vashaee, D. et al. High-thermoelectric performance of nanostructured bismuth antimony telluride bulk alloys. *Science* **2008**, *320*, 634–638.

[113] Ghaemi, P.; Mong, R. S. K.; Moore, J. E. In-plane transport and enhanced thermoelectric performance in thin films of the topological insulators Bi$_2$Te$_3$ and Bi$_2$Se$_3$. *Phys. Rev. Lett.* **2010**, *105*, 166603.

[114] Toriyama, M. Y.; Snyder, G. J. Are topological insulators promising thermoelectrics. *Mater. Horiz.* **2024**, *11*, 1188–1198.

[115] Linder, J.; Yokoyama, T.; Sudbø, A. Anomalous finite size effects on surface states in the topological insulator Bi$_2$Se$_3$. *Phys. Rev. B: Condens. Matter Mater. Phys.* **2009**, *80*, 205401.

[116] Roth, A.; Brüne, C.; Buhmann, H.; Molenkamp, L. W.; Maciejko, J.; Qi, X. L.; Zhang, S. C. Nonlocal transport in the quantum spin Hall state. *Science* **2009**, *325*, 294–297.

[117] Fu, L.; Kane, C. L. Superconducting proximity effect and Majorana fermions at the surface of a topological insulator. *Phys. Rev. Lett.* **2008**, *100*, 096407.

[118] Schmitt, T. W.; Connolly, M. R.; Schleenvoigt, M.; Liu, C. L.; Kennedy, O.; Chávez-Garcia, J. M.; Jalil, A. R.; Bennemann, B.; Trellenkamp, S.; Lentz, F. et al. Integration of topological insulator Josephson junctions in superconducting qubit circuits. *Nano Lett.* **2022**, *22*, 2595–2602.

[119] Sun, H. H.; Jia, J. F. Detection of Majorana zero mode in the vortex. *npj Quantum Mater.* **2017**, *2*, 34.

[120] Wiedenmann, J.; Bocquillon, E.; Deacon, R. S.; Hartinger, S.; Herrmann, O.; Klapwijk, T. M.; Maier, L.; Ames, C.; Brüne, C.; Gould, C. et al. 4π-periodic Josephson supercurrent in HgTe-based topological Josephson junctions. *Nat. Commun.* **2016**, *7*, 10303.

[121] Schüffelgen, P.; Rosenbach, D.; Li, C.; Schmitt, T. W.; Schleenvoigt, M.; Jalil, A. R.; Schmitt, S.; Kölzer, J.; Wang, M.; Bennemann, B. et al. Selective area growth and stencil lithography for *in situ* fabricated quantum devices. *Nat. Nanotechnol.* **2019**, *14*, 825–831.

[122] Sarma, S. D.; Freedman, M.; Nayak, C. Majorana zero modes and topological quantum computation. *npj Quantum Inf.* **2015**, *1*, 15001.

[123] Xu, J. P.; Wang, M. X.; Liu, Z. L.; Ge, J. F.; Yang, X. J.; Liu, C. H.; Xu, Z. A.; Guan, D. D.; Gao, C. L.; Qian, D. et al. Experimental detection of a Majorana mode in the core of a magnetic vortex inside a topological insulator-superconductor Bi$_2$Te$_3$/NbSe$_2$ heterostructure. *Phys. Rev. Lett.* **2015**, *114*, 017001.

[124] Flötotto, D.; Ota, Y.; Bai, Y.; Zhang, C.; Okazaki, K.; Tsuzuki, A.; Hashimoto, T.; Eckstein, J. N.; Shin, S.; Chiang, T. C. Superconducting pairing of topological surface states in bismuth selenide films on niobium. *Sci. Adv.* **2018**, *4*, eaar7214.

[125] Wang, M. X.; Liu, C. H.; Xu, J. P.; Yang, F.; Miao, L.; Yao, M. Y.; Gao, C. L.; Shen, C. Y.; Ma, X. C.; Chen, X. et al. The coexistence of superconductivity and topological order in the Bi$_2$Se$_3$ thin films. *Science* **2012**, *336*, 52–55.

[126] Hsieh, D.; Wray, L.; Qian, D.; Xia, Y.; Dil, J. H.; Meier, F.; Patthey, L.; Osterwalder, J.; Bihlmayer, G.; Hor, Y. S. et al. Direct observation of spin-polarized surface states in the parent compound of a topological insulator using spin- and angle-resolved photoemission spectroscopy in a Mott-polarimetry mode. *New J. Phys.* **2010**, *12*, 125001.

[127] Hasan, M. Z.; Moore, J. E. Three-dimensional topological insulators. *Annu. Rev. Condens. Matter Phys.* **2011**, *2*, 55–78.

[128] Neupane, M.; Richardella, A.; Sánchez-Barriga, J.; Xu, S. Y.; Alidoust, N.; Belopolski, I.; Liu, C.; Bian, G.; Zhang, D. M.; Marchenko, D. et al. Observation of quantum-tunnelling-modulated spin texture in ultrathin topological insulator Bi$_2$Se$_3$ films. *Nat. Commun.* **2014**, *5*, 3841.

[129] Reis, F.; Li, G.; Dudy, L.; Bauernfeind, M.; Glass, S.; Hanke, W.; Thomale, R.; Schäfer, J.; Claessen, R. Bismuthene on a SiC substrate: A candidate for a high-temperature quantum spin Hall material. *Science* **2017**, *357*, 287–290.

[130] Lüpke, F.; Just, S.; Eschbach, M.; Heider, T.; Młyńczak, E.; Lanius, M.; Schüffelgen, P.; Rosenbach, D.; Von Den Driesch, N.; Cherepanov, V. et al. In situ disentangling surface state transport channels of a topological insulator thin film by gating. *npj Quantum Mater.* **2018**, *3*, 46.

[131] Leis, A.; Schleenvoigt, M.; Cherepanov, V.; Lüpke, F.; Schüffelgen, P.; Mussler, G.; Grützmacher, D.; Voigtländer, B.; Tautz, F. S. Lifting the spin-momentum locking in ultra-thin topological insulator films. *Adv. Quantum Technol.* **2021**, *4*, 2100083.

[132] Leis, A.; Schleenvoigt, M.; Moors, K.; Soltner, H.; Cherepanov, V.; Schüffelgen, P.; Mussler, G.; Grützmacher, D.; Voigtländer, B.; Lüpke, F. et al. Probing edge state conductance in ultra-thin topological insulator films. *Adv. Quantum Technol.* **2022**, *5*, 2200043.

[133] Zhang, Y.; He, K.; Chang, C. Z.; Song, C. L.; Wang, L. L.; Chen, X.; Jia, J. F.; Fang, Z.; Dai, X.; Shan, W. Y. et al. Crossover of the three-dimensional topological insulator Bi$_2$Se$_3$ to the two-dimensional limit. *Nat. Phys.* **2010**, *6*, 584–588.

[134] Zhang, J.; Peng, Z. P.; Soni, A.; Zhao, Y. Y.; Xiong, Y.; Peng, B.; Wang, J. B.; Dresselhaus, M. S.; Xiong, Q. H. Raman spectroscopy of few-quintuple layer topological insulator Bi$_2$Se$_3$ nanoplatelets. *Nano Lett.* **2011**, *11*, 2407–2414.

[135] Harpeness, R.; Gedanken, A. Microwave-assisted synthesis of nanosized Bi$_2$Se$_3$. *New J. Chem.* **2003**, *27*, 1191–1193.

[136] Hu, P. F.; Cao, Y. L.; Jia, D. Z.; Wang, L. X. Selective synthesis of Bi$_2$Se$_3$ nanostructures by solvothermal reaction. *Mater. Lett.* **2010**, *64*, 493–496.

[137] Kadel, K.; Kumari, L.; Li, W. Z.; Huang, J. Y.; Provencio, P. P. Synthesis and thermoelectric properties of Bi$_2$Se$_3$ nanostructures. *Nanoscale Res. Lett.* **2011**, *6*, 57.

[138] Wei, T. X.; Zhang, Y.; Dong, W. J.; Huang, C. Y.; Sun, Y.; Chen, X.; Dai, N. A solution synthetic route toward Bi$_2$Se$_3$ layered nanostructures with tunable thickness via weakening precursor reactivity. *Phys. Status Solidi A* **2013**, *210*, 1909–1913.

[139] Park, Y. S.; Lee, J. S. Synthesis of single-crystalline topological insulator Bi$_2$Se$_3$ nanomaterials with various morphologies. *J. Nanoparticle Res.* **2014**, *16*, 2226.

[140] Xu, H. M.; Chen, G.; Jin, R. C.; Chen, D. H.; Wang, Y.; Pei, J.; Zhang, Y. Q.; Yan, C. S.; Qiu, Z. Z. Microwave-assisted synthesis of Bi$_2$Se$_3$ ultrathin nanosheets and its electrical conductivities. *CrystEngComm,* **2014**, *16*, 3965–3970.

[141] Min, Y.; Park, G.; Kim, B.; Giri, A.; Zeng, J.; Roh, J. W.; Kim, S. I.; Lee, K. H.; Jeong, U. Synthesis of multishell nanoplates by consecutive epitaxial growth of Bi$_2$Se$_3$ and Bi$_2$Te$_3$ nanoplates and enhanced thermoelectric properties. *ACS Nano* **2015**, *9*, 6843–6853.

[142] Buchenau, S.; Akinsinde, L. O.; Zocher, M.; Rukser, D.; Schürmann, U.; Kienle, L.; Grimm-Lebsanft, B.; Rübhausen, M. Scalable polyol synthesis for few quintuple layer thin and ultra high aspect ratio Bi$_2$Se$_3$ structures. *Solid State Commun.* **2018**, *281*, 49–52.

[143] Pradhan, B.; Dalui, A.; Paul, S.; Roy, D.; Acharya, S. Solution phase synthesis of large-area ultra-thin two dimensional layered Bi$_2$Se$_3$: Role of Cu-intercalation and substitution. *Mater. Res. Express* **2020**, *6*, 124005.

[144] Masood, K. B.; Kumar, P.; Giri, R.; Singh, J. Controlled synthesis of two-dimensional (2D) ultra-thin bismuth selenide (Bi$_2$Se$_3$) nanosheets by bottom-up solution-phase chemistry and its electrical transport properties for thermoelectric application. *FlatChem* **2020**, *21*, 100165.

[145] Samanta, M.; Biswas, K. 2D nanosheets of topological quantum materials from homologous $(Bi_2)_m(Bi_2Se_3)_n$ heterostructures: Synthesis and ultralow thermal conductivity. *Chem. Mater.* **2020**, *32*, 8819–8826.

[146] Maiti, P. S.; Ghosh, S.; Leitus, G.; Houben, L.; Bar Sadan, M. Oriented attachment of 2D nanosheets: The case of few-layer Bi$_2$Se$_3$. *Chem. Mater.* **2021**, *33*, 7558–7565.

[147] Mazumder, K.; Shirage, P. M. A brief review of Bi$_2$Se$_3$ based topological insulator: From fundamentals to applications. *J. Alloys Compd.* **2021**, *888*, 161492.

[148] Jurczyszyn, M.; Sikora, M.; Chrobak, M.; Jurczyszyn, L. Studies of

surface states in Bi$_2$Se$_3$ induced by the Bi$_{Se}$ substitution in the crystal subsurface structure. *Appl. Surf. Sci.* **2020**, *58*, 146978.

[149] Wang, Y. L.; Jiang, Y. P.; Chen, M.; Li, Z.; Song, C. L.; Wang, L. L.; He, K.; Chen, X.; Ma, X. C.; Xue, Q. K. Scanning tunneling microscopy of interface properties of Bi$_2$Se$_3$ on FeSe. *J. Phys.: Condens. Matter* **2012**, *24*, 475604.

[150] Zhang, T.; Levy, N.; Ha, J.; Kuk, Y.; Stroscio, J. A. Scanning tunneling microscopy of gate tunable topological insulator Bi$_2$Se$_3$ thin films. *Phys. Rev. B: Condens. Matter Mater. Phys.* **2013**, *87*, 115410.

[151] Stroscio, J. A.; Feenstra, R. M.; Fein, A. P. Electronic structure of the Si(111)2×1 surface by scanning-tunneling microscopy. *Phys. Rev. Lett.* **1986**, *57*, 2579–2582.

[152] Li, T. X.; Wang, P. J.; Fu, H. L.; Du, L. J.; Schreiber, K. A.; Mu, X. Y.; Liu, X. X.; Sullivan, G.; Csáthy, G. A.; Lin, X. et al. Observation of a helical Luttinger liquid in InAs/GaSb quantum spin Hall edges. *Phys. Rev. Lett.* **2015**, *115*, 136804.

[153] Zhang, S. B.; Zhang, Y. Y.; Shen, S. Q. Robustness of quantum spin Hall effect in an external magnetic field. *Phys. Rev. B* **2014**, *90*, 115305.

[154] Knez, I.; Du, R. R.; Sullivan, G. Evidence for helical edge modes in inverted InAs/GaSb quantum wells. *Phys. Rev. Lett.* **2011**, *107*, 136603.

[155] Knez, I.; Rettner, C. T.; Yang, S. H.; Parkin, S. S. P.; Du, L. J.; Du, R. R.; Sullivan, G. Observation of edge transport in the disordered regime of topologically insulating InAs/GaSb quantum wells. *Phys. Rev. Lett.* **2014**, *112*, 026602.

[156] Du, L. J.; Knez, I.; Sullivan, G.; Du, R. R. Robust helical edge transport in gated InAs/GaSb bilayers. *Phys. Rev. Lett.* **2015**, *114*, 096802.

[157] Jäck, B.; Xie, Y. L.; Andrei Bernevig, B.; Yazdani, A. Observation of backscattering induced by magnetism in a topological edge state. *Proc. Natl. Acad. Sci. USA.* **2020**, *117*, 16214–16218.

[158] Song, C. L.; Wang, L. L.; He, K.; Ji, S. H.; Chen, X.; Ma, X. C.; Xue, Q. K. Probing Dirac fermion dynamics in topological insulator Bi$_2$Se$_3$ films with a scanning tunneling microscope. *Phys. Rev. Lett.* **2015**, *114*, 176602.

[159] Wang, J.; DaSilva, A. M.; Chang, C. Z.; He, K.; Jain, J. K.; Samarth, N.; Ma, X. C.; Xue, Q. K.; Chan, M. H. W. Evidence for electron–electron interaction in topological insulator thin films. *Phys. Rev. B: Condens. Matter Mater. Phys.* **2011**, *83*, 245438.

[160] Kong, D. S.; Dang, W. H.; Cha, J. J.; Li, H.; Meister, S.; Peng, H. L.; Liu, Z. F.; Cui, Y. Few-layer nanoplates of Bi$_2$Se$_3$ and Bi$_2$Te$_3$ with highly tunable chemical potential. *Nano Lett.* **2010**, *10*, 2245–2250.

[161] Min, Y.; Roh, J. W.; Yang, H.; Park, M.; Kim, S. I.; Hwang, S.; Lee, S. M.; Lee, K. H.; Jeong, U. Surfactant-free scalable synthesis of Bi$_2$Te$_3$ and Bi$_2$Se$_3$ nanoflakes and enhanced thermoelectric properties of their nanocomposites. *Adv. Mater.* **2013**, *25*, 1424–1424.

[162] Son, J. S.; Choi, M. K.; Han, M. K.; Park, K.; Kim, J. Y.; Lim, S. J.; Oh, M.; Kuk, Y.; Park, C.; Kim, S. J. et al. n-Type nanostructured thermoelectric materials prepared from chemically synthesized ultrathin Bi$_2$Te$_3$ nanoplates. *Nano Lett.* **2012**, *12*, 640–647.

[163] Zhang, G. Q.; Wang, W.; Lu, X. L.; Li, X. G. Solvothermal synthesis of V-VI binary and ternary hexagonal platelets: The oriented attachment mechanism. *Cryst. Growth Des.* **2009**, *9*, 145–150.

[164] Zeljkovic, I.; Okada, Y.; Huang, C. Y.; Sankar, R.; Walkup, D.; Zhou, W. W.; Serbyn, M.; Chou, F. C.; Tsai, W. F.; Lin, H. et al. Mapping the unconventional orbital texture in topological crystalline insulators. *Nat. Phys.* **2014**, *10*, 572–577.

[165] Guo, H.; Yan, C. H.; Liu, J. W.; Wang, Z. Y.; Wu, R.; Zhang, Z. D.; Wang, L. L.; He, K.; Ma, X. C.; Ji, S. H. et al. Topological crystalline insulator Pb$_x$Sn$_{1-x}$Te thin films on SrTiO$_3$(001) with tunable Fermi levels. *APL Mater.* **2014**, *2*, 056106.

[166] Pletikosić, I.; Gu, G. D.; Valla, T. Inducing a Lifshitz transition by extrinsic doping of surface bands in the topological crystalline insulator Pb$_{1-x}$Sn$_x$Se. *Phys. Rev. Lett.* **2014**, *112*, 146403.

[167] Zhang, D. M.; Baek, H.; Ha, J.; Zhang, T.; Wyrick, J.; Davydov, A. V.; Kuk, Y.; Stroscio, J. A. Quasiparticle scattering from topological crystalline insulator SnTe(001) surface states. *Phys. Rev. B* **2014**, *89*, 245445.

[168] Safdar, M.; Wang, Q. S.; Wang, Z. X.; Zhan, X. Y.; Xu, K.; Wang, F. M.; Mirza, M.; He, J. Weak antilocalization effect of topological crystalline insulator Pb$_{1-x}$Sn$_x$Te nanowires with tunable composition and distinct {100} facets. *Nano Lett.* **2015**, *15*, 2485–2490.

[169] Yan, C. H.; Liu, J. W.; Zang, Y. Y.; Wang, J. F.; Wang, Z. Y.; Wang, P.; Zhang, Z. D.; Wang, L. L.; Ma, X. C.; Ji, S. H. et al. Experimental observation of Dirac-like surface states and topological phase transition in Pb$_{1-x}$Sn$_x$Te(111) films. *Phys. Rev. Lett.* **2014**, *112*, 186801.

[170] Neupane, M.; Xu, S. Y.; Sankar, R.; Gibson, Q.; Wang, Y. J.; Belopolski, I.; Alidoust, N.; Bian, G.; Shibayev, P. P.; Sanchez, D. S. et al. Topological phase diagram and saddle point singularity in a tunable topological crystalline insulator. *Phys. Rev. B* **2015**, *92*, 075131.

[171] Assaf, B. A.; Phuphachong, T.; Volobuev, V. V.; Inhofer, A.; Bauer, G.; Springholz, G.; De Vaulchier, L. A.; Guldner, Y. Massive and massless Dirac fermions in Pb$_{1-x}$Sn$_x$Te topological crystalline insulator probed by magneto-optical absorption. *Sci. Rep.* **2016**, *6*, 20323.

[172] Wang, Y.; Luo, G. Y.; Liu, J. W.; Sankar, R.; Wang, N. L.; Chou, F. C.; Fu, L.; Li, Z. Q. Observation of ultrahigh mobility surface states in a topological crystalline insulator by infrared spectroscopy. *Nat. Commun.* **2017**, *8*, 366.

[173] Krizman, G.; Assaf, B. A.; Phuphachong, T.; Bauer, G.; Springholz, G.; Bastard, G.; Ferreira, R.; De Vaulchier, L. A.; Guldner, Y. Tunable Dirac interface states in topological superlattices. *Phys. Rev. B* **2018**, *98*, 075303.

[174] Turowski, B.; Kazakov, A.; Rudniewski, R.; Sobol, T.; Partyka-Jankowska, E.; Wojciechowski, T.; Aleszkiewicz, M.; Zaleszczyk, W.; Szczepanik, M.; Wojtowicz, T. et al. Spin-polarization of topological crystalline and normal insulator Pb$_{1-x}$Sn$_x$Se(111) epilayers probed by photoelectron spectroscopy. *Appl. Surf. Sci.* **2023**, *610*, 155434.

[175] Wang, J. S.; Liu, X. Y.; Wang, T. Y.; Ozerov, M.; Assaf, B. A. *g* factor of topological interface states in Pb$_{1-x}$Sn$_x$Se quantum wells. *Phys. Rev. B* **2023**, *107*, 155307.

[176] Brzezicki, W.; Wysokiński, M. M.; Hyart, T. Topological properties of multilayers and surface steps in the SnTe material class. *Phys. Rev. B* **2019**, *100*, 121107.

[177] Du, H.; Chen, C. A. L.; Krishnan, R.; Krauss, T. D.; Harbold, J. M.; Wise, F. W.; Thomas, M. G.; Silcox, J. Optical properties of colloidal PbSe nanocrystals. *Nano Lett.* **2002**, *2*, 1321–1324.

[178] Wehrenberg, B. L.; Wang, C. J.; Guyot-Sionnest, P. Interband and intraband optical studies of PbSe colloidal quantum dots. *J. Phys. Chem. B* **2002**, *106*, 10634–10640.

[179] Schaller, R. D.; Petruska, M. A.; Klimov, V. I. Tunable near-infrared optical gain and amplified spontaneous emission using PbSe nanocrystals. *J. Phys. Chem. B* **2003**, *107*, 13765–13768.

[180] Allan, G.; Delerue, C. Confinement effects in PbSe quantum wells and nanocrystals. *Phys. Rev. B: Condens. Matter Mater. Phys.* **2004**, *70*, 245321.

[181] Hens, Z.; Vanmaekelbergh, D.; Kooij, E. S.; Wormeester, H.; Allan, G.; Delerue, C. Effect of quantum confinement on the dielectric function of PbSe. *Phys. Rev. Lett.* **2004**, *92*, 026808.

[182] Liljeroth, P.; Van Emmichoven, P. A. Z.; Hickey, S. G.; Weller, H.; Grandidier, B.; Allan, G.; Vanmaekelbergh, D. Density of states measured by scanning-tunneling spectroscopy sheds new light on the optical transitions in PbSe nanocrystals. *Phys. Rev. Lett.* **2005**, *95*, 086801.

[183] Koole, R.; Allan, G.; Delerue, C.; Meijerink, A.; Vanmaekelbergh, D.; Houtepen, A. J. Optical investigation of quantum confinement in PbSe nanocrystals at different points in the Brillouin zone. *Small* **2008**, *4*, 127–133.

[184] Petkov, V.; Moreels, I.; Hens, Z.; Ren, Y. PbSe quantum dots: Finite, off-stoichiometric, and structurally distorted. *Phys. Rev. B: Condens. Matter Mater. Phys.* **2010**, *81*, 241304.

[185] Peters, J. L.; Van Den Bos, K. H. W.; Van Aert, S.; Goris, B.; Bals, S.; Vanmaekelbergh, D. Ligand-induced shape transformation of PbSe nanocrystals. *Chem. Mater.* **2017**, *29*, 4122–4128.

[186] Evers, W. H.; Goris, B.; Bals, S.; Casavola, M.; De Graaf, J.; Van Roij, R.; Dijkstra, M.; Vanmaekelbergh, D. Low-dimensional semiconductor superlattices formed by geometric control over nanocrystal attachment. *Nano Lett.* **2013**, *13*, 2317–2323.

[187] Wang, Y.; Peng, X. X.; Abelson, A.; Xiao, P. H.; Qian, C. R. O. L. N.; Yu, L.; Ophus, C.; Ercius, P.; Wang, L. W.; Law, M. et al. Dynamic deformability of individual PbSe nanocrystals during superlattice phase transitions. *Sci. Adv.* **2019**, *5*, 5623.

[188] Whitham, K.; Smilgies, D. M.; Hanrath, T. Entropic, enthalpic, and kinetic aspects of interfacial nanocrystal superlattice assembly and attachment. *Chem. Mater.* **2018**, *30*, 54–63.

[189] McCray, A. R. C.; Savitzky, B. H.; Whitham, K.; Hanrath, T.; Kourkoutis, L. F. Orientational disorder in epitaxially connected quantum dot solids. *ACS Nano* **2019**, *13*, 11460–11468.

[190] Whitham, K.; Yang, J.; Savitzky, B. H.; Kourkoutis, L. F.; Wise, F.; Hanrath, T. Charge transport and localization in atomically coherent quantum dot solids. *Nat. Mater.* **2016**, *15*, 557–563.

[191] Salzmann, B. B. V.; Van Der Sluijs, M. M.; Soligno, G.; Vanmaekelbergh, D. Oriented attachment: From natural crystal growth to a materials engineering tool. *Acc. Chem. Res.* **2021**, *54*, 787–797.

[192] Yalcin, A. O.; Fan, Z. C.; Goris, B.; Li, W. F.; Koster, R. S.; Fang, C. M.; Van Blaaderen, A.; Casavola, M.; Tichelaar, F. D.; Bals, S. et al. Atomic resolution monitoring of cation exchange in CdSe–PbSe heteronanocrystals during epitaxial solid-solid-vapor growth. *Nano Lett.* **2014**, *14*, 3661–3667.

[193] Son, D. H.; Hughes, S. M.; Yin, Y. D.; Paul Alivisatos, A. Cation exchange reactions in ionic nanocrystals. *Science* **2004**, *306*, 1009–1012.

[194] Lambert, K.; Geyter, B. D.; Moreels, I.; Hens, Z. PbTe–CdTe core–shell particles by cation exchange, a HR-TEM study. *Chem. Mater.* **2009**, *21*, 778–780.

[195] Li, H. B.; Zanella, M.; Genovese, A.; Povia, M.; Falqui, A.; Giannini, C.; Manna, L. Sequential cation exchange in nanocrystals: Preservation of crystal phase and formation of metastable phases. *Nano Lett.* **2011**, *11*, 4964–4970.

[196] Bouet, C.; Laufer, D.; Mahler, B.; Nadal, B.; Heuclin, H.; Pedetti, S.; Patriarche, G.; Dubertret, B. Synthesis of zinc and lead chalcogenide core and core/shell nanoplatelets using sequential cation exchange reactions. *Chem. Mater.* **2014**, *26*, 3002–3008.

[197] Justo, Y.; Sagar, L. K.; Flamee, S.; Zhao, Q.; Vantomme, A.; Hens, Z. Less is more. Cation exchange and the chemistry of the nanocrystal surface. *ACS Nano* **2014**, *8*, 7948–7957.

[198] Meir, N.; Martín-García, B.; Moreels, I.; Oron, D. Revisiting the anion framework conservation in cation exchange processes. *Chem. Mater.* **2016**, *28*, 7872–7877.

[199] Makké, L.; Fu, N. Y.; Lehouelleur, H.; Po, H.; Dabard, C.; Curti, L.; Bossavit, E.; Xu, X. Z.; Patriarche, G.; Pierucci, D. et al. Impact of the surface chemistry of 2D nanoplatelets on cation exchange. *Chem. Mater.* **2023**, *35*, 9581–9590.

[200] Lannoo, M.; Prins, P. T.; Hens, Z.; Vanmaekelbergh, D.; Delerue, C. Universality of optical absorptance quantization in two-dimensional group-IV, III-V, II-VI, and IV-VI semiconductors. *Phys. Rev. B* **2022**, *105*, 035421.

[201] Moreels, I.; Lambert, K.; Smeets, D.; De Muynck, D.; Nollet, T.; Martins, J. C.; Vanhaecke, F.; Vantomme, A.; Delerue, C.; Allan, G. et al. Size-dependent optical properties of colloidal PbS quantum dots. *ACS Nano* **2009**, *3*, 3023–3030.

[202] Kang, I.; Wise, F. W. Electronic structure and optical properties of PbS and PbSe quantum dots. *J. Opt. Soc. Am. B,* **1997**, *14*, 1632–1646.

[203] Wise, F. W. Lead salt quantum dots: The limit of strong quantum confinement. *Acc. Chem. Res.* **2000**, *33*, 773–780.

[204] Beard, M. C.; Luther, J. M.; Semonin, O. E.; Nozik, A. J. Third generation photovoltaics based on multiple exciton generation in quantum confined semiconductors. *Acc. Chem. Res.* **2013**, *46*, 1252–1260.

[205] Gao, J. B.; Jeong, S.; Lin, F.; Erslev, P. T.; Semonin, O. E.; Luther, J. M.; Beard, M. C. Improvement in carrier transport properties by mild thermal annealing of PbS quantum dot solar cells. *Appl. Phys. Lett.* **2013**, *102*, 043506.

[206] Beard, M. C.; Luther, J. M.; Nozik, A. J. The promise and challenge of nanostructured solar cells. *Nat. Nanotechnol.* **2014**, *9*, 951–954.

[207] Drüppel, M.; Krüger, P.; Rohlfing, M. Strain tuning of Dirac states at the SnTe (001) surface. *Phys. Rev. B* **2014**, *90*, 155312.

[208] Safdar, M.; Wang, Q. S.; Mirza, M.; Wang, Z. X.; He, J. Crystal shape engineering of topological crystalline insulator SnTe microcrystals and nanowires with huge thermal activation energy gap. *Cryst. Growth Des.* **2014**, *14*, 2502–2509.

[209] Shen, J.; Jung, Y.; Disa, A. S.; Walker, F. J.; Ahn, C. H.; Cha, J. J. Synthesis of SnTe nanoplates with {100} and {111} surfaces. *Nano Lett.* **2014**, *14*, 4183–4188.

[210] Schapotschnikow, P.; Van Huis, M. A.; Zandbergen, H. W.; Vanmaekelbergh, D.; Vlugt, T. J. H. Morphological transformations and fusion of PbSe nanocrystals studied using atomistic simulations. *Nano Lett.* **2010**, *10*, 3966–3971.

[211] Kazakov, A.; Brzezicki, W.; Hyart, T.; Turowski, B.; Polaczyński, J.; Adamus, Z.; Aleszkiewicz, M.; Wojciechowski, T.; Domagala, J. Z.; Caha, O. et al. Signatures of dephasing by mirror-symmetry breaking in weak-antilocalization magnetoresistance across the topological transition in Pb$_{1-x}$Sn$_x$Se. *Phys. Rev. B* **2021**, *103*, 245307.

[212] He, F. G.; Klein, E.; Bartling, S.; Saeidpour, S.; Corzilius, B.; Lesyuk, R.; Klinke, C. Template-mediated formation of colloidal two-dimensional tin telluride nanosheets and the role of the ligands. *J. Phys. Chem. C* **2022**, *126*, 20498–20504.

[213] Li, F.; Fu, J. C.; Torche, A.; Kull, S.; Kornowski, A.; Lesyuk, R.; Bester, G.; Klinke, C. Single-crystalline colloidal quasi-2D tin telluride. *Adv. Mater. Interfaces* **2020**, *7*, 2000410.

[214] Wang, Q. S.; Wang, F.; Li, J.; Wang, Z. X.; Zhan, X. Y.; He, J. Low-dimensional topological crystalline insulators. *Small* **2015**, *11*, 4613–4624.

[215] Liu, P. Z.; Williams, J. R.; Cha, J. J. Topological nanomaterials. *Nat. Rev. Mater.* **2019**, *4*, 479–496.

[216] Liu, C. W.; Wang, Z. H.; Qiu, R. L. J.; Gao, X. P. A. Development of topological insulator and topological crystalline insulator nanostructures. *Nanotechnology* **2020**, *31*, 192001.

[217] Arachchige, I. U.; Kanatzidis, M. G. Anomalous band gap evolution from band inversion in Pb$_{1-x}$Sn$_x$Te nanocrystals. *Nano Lett.* **2009**, *9*, 1583–1587.

[218] Wei, H.; Chen, S. Z.; Ren, X. L.; Qian, B. J.; Su, Y. J.; Yang, Z.; Zhang, Y. F. Band gap tunable Sn-doped PbSe nanocrystals: Solvothermal synthesis and first-principles calculations. *CrystEngComm* **2012**, *14*, 7408–7414.

[219] Vinoth, S.; Karthikeyan, V.; Roy, V. A. L.; Srinivasan, B.; Thilakan, P. Bismuth telluride (Bi$_2$Te$_3$) nanocrystallites: Studies on growth morphology and its influence on the thermoelectric properties. *J. Cryst. Growth* **2023**, *606*, 127087.